



NASA TM-80183

NASA Technical Memorandum 80183

NASA-TM-80183 19800004567

DO NOT REMOVE FROM THIS ROOM

EXPERIMENTAL AND NUMERICAL RESULTS ON A SHEAR LAYER EXCITED BY A SOUND PULSE

LUCIO MAESTRELLO
ALVIN BAYLISS
ELI TURKEL

NOVEMBER 1979



National Aeronautics and
Space Administration

Langley Research Center
Hampton, Virginia 23665

LIBRARY COPY

1979

LANGLEY RESEARCH CENTER
LIBRARY, NASA
HAMPTON, VIRGINIA

SUMMARY

The behavior of a sound in a jet is investigated both experimentally and numerically. It is verified that the far-field acoustic power increases with flow velocity for the lower and medium frequency range. Experimentally, an attenuation at higher frequencies is also observed. This increase is found numerically to be due primarily to the interaction between the mean vorticity and the fluctuation velocities. Spectral decomposition of the real time data indicates that the power increase occurs in the low and middle frequency range, where the local instability waves have the largest spatial growth rate. The connection between this amplification and the local instability waves is discussed.

INTRODUCTION

The purpose of this paper is to study the interaction of an acoustic disturbance with a jet, both numerically and experimentally. An attempt will be made to clarify the role of the shear interaction terms in the overall sound pattern. The Lighthill acoustic analogy (refs. 1 and 2) accounts for this interaction in principle, since it includes as source terms on the right hand side all of the interaction terms in the Navier-Stokes equations. However, the Lighthill theory requires prior knowledge of the solution in order to specify the sources.

Lighthill did point out, however, that jet noise may be amplified by shear interaction terms (ref. 2). At present, this phenomenon has not been satisfactorily analyzed. In fact, it may not be adequately resolved for

some time, since complete specification of the Lighthill source terms requires a solution of the Navier-Stokes equations with turbulence. However, much progress has been made since the publication of the Lighthill analogy.

The first modification of the Lighthill formulation was by Phillips (ref. 3) who shifted some convection terms from the right hand side to the left hand side, resulting in a second order convective wave equation. As pointed out by Doak (ref. 4), the Phillips formulation does not account for all of the first order interaction terms between the fluctuating and mean fields. However, these terms are not generally considered important at the higher frequencies where refraction predominates (ref. 4).

A further extension of the Lighthill theory was obtained by Lilley (ref. 5). Lilley developed as his propagation operator (i.e. as his left hand side) a third order wave-like equation which explicitly accounts for all of the first order interaction terms between the fluctuating and the mean fields, including the shear interaction terms. The left hand side of the Lilley equation is nothing but the Orr-Sommerfeld equation for the stability of the mean flow and in fact is equivalent to the Euler equations, linearized about the mean flow.

Several authors have studied the Lilley equation. Most of these studies have been restricted to a parallel, transversely sheared mean flow. Tester and Morfey (ref. 6), for example, obtained both numerical and analytical results with sources modelled by quadrupoles. They computed a strong amplification at mid angles from the jet axis due to the shear interaction. This work was restricted to parallel mean flows. Mungur et al (ref. 7), on the other hand, studied the Euler equations linearized about a spreading jet,

using a semi-analytical approach. They divided the region into spherical shells and obtained a sequence of directivity modes in each shell. A difficulty of this method is that it is not clear how to match the solution between shells and thus obtain the solution due to a given source on the right hand side.

Further studies of the shear interaction terms were done by using a vortex sheet model for the mean flow. In this model, the shear interaction terms are replaced by jump conditions at the interface. This model has been studied with both fixed and moving sources. As the disturbance interacts with the vortex sheet, the vortex sheet becomes unstable (Miles ref. 8, Ribner ref. 9, Mani ref. 10, and Dowling et al ref. 11). It has been shown that such an instability can lead to significant amplification of sound in supersonic flow. This is especially true when the acoustic coupling between opposite sides of the vortex sheet becomes large (Howe ref. 12). These studies were restricted to parallel or weakly nonparallel flows. Morris and Tam (ref. 13) have also computed the far-field acoustic sound from instability waves in a supersonic, spreading jet using the method of matched asymptotic expansions.

Experiments by Vlasov and Givensky (ref.14) have shown that local instability waves in a jet can be excited by acoustic disturbances. This was confirmed analytically by Tam (ref. 15). Moore (ref. 16) and Bechert and Pfizenmaier (ref. 17) have shown that broadband sound can be increased when a jet is excited by an acoustic wave impinging from upstream of the nozzle. Kibens (ref. 18) acoustically excited the jet at the tip of the nozzle and also obtained an increase in the far-field sound accompanied by a near-field pulsation of the jet. These results support the conjecture that instability waves can significantly amplify sound.

In the present paper, the effect of the flow on the total power output of an acoustic source in the potential core of the jet will be considered. Since only the result of the interaction between the acoustic field and the jet is to be studied, no attempt will be made to model the real sources of the jet. It will be shown both numerically and experimentally that significant increase in power output occurs at low frequencies where the instability waves are known to have the largest growth rate (refs. 19 and 20).

The numerical simulation will be obtained by solving the full, time dependent Euler equations, linearized about a realistic spreading jet. These equations contain all of the first order interaction terms between the acoustic field and the mean flow. This permits computation of a more complete interaction than can be obtained from computations of classical refraction effects (refs. 21 and 22).

In section 2, the governing equations are introduced. Details of the numerical scheme and the numerical boundary conditions are given in sections 3 and 4. In section 5, the experimental configuration is described. Results and discussion are presented in section 6.

II. GOVERNING EQUATIONS

The equations of fluid flow can be written as a first order system

$$\frac{\partial \rho}{\partial t} + \text{div}(\rho \vec{v}) = 0 \quad (2.1)$$

$$\rho \left(\frac{\partial v_i}{\partial t} + v_j \frac{\partial v_i}{\partial y_j} \right) + \frac{\partial p}{\partial y_i} = \frac{\partial e_{ij}}{\partial y_j}$$

Here ρ is the density, \vec{v} the velocity, p is the pressure and e_{ij} the viscous stress tensor. In the system (eq. (2.1)), use is made of the summation convention on repeated indices.

We now divide the flow variables into mean and fluctuating parts. We thus write

$$\rho = \bar{\rho} + \rho'$$

$$\vec{v} = \vec{\bar{U}} + \vec{u}'$$

$$p = \bar{p} + p'$$

where the bar denotes a mean quantity independent of time.

We can thus rewrite equation (2.1) as a system for the fluctuating quantities along

$$\begin{aligned} \frac{\partial \rho'}{\partial t} + \text{div}(\rho' \vec{\bar{U}}) + \text{div}(\bar{\rho} \vec{u}') &= -\text{div}(\bar{\rho} \vec{\bar{U}}) - \text{div}(\rho' \vec{u}') \\ \bar{\rho} \frac{\partial u'_i}{\partial t} + \bar{U}_j \frac{\partial u'_{ij}}{\partial y_j} + u'_j \frac{\partial \bar{U}_i}{\partial y_j} + \rho' \bar{U}_j \frac{\partial \bar{U}_i}{\partial y_j} + \frac{\partial p'}{\partial y_i} &= \\ \frac{\partial e_{ij}}{\partial y_j} - \frac{\partial \bar{p}}{\partial y_i} - \bar{\rho} \bar{U}_j \frac{\partial \bar{U}_i}{\partial y_j} - \rho u'_j \frac{\partial u'_i}{\partial y_j} - & \\ -\rho' \left(\frac{\partial u'_i}{\partial t} + \bar{U}_j \frac{\partial u'_i}{\partial y_j} + u'_j \frac{\partial \bar{U}_i}{\partial y_j} \right) & \\ \rho' \left(\bar{U}_j \frac{\partial u'_i}{\partial y_j} + u'_j \frac{\partial \bar{U}_i}{\partial y_j} + \frac{\partial u'_i}{\partial t} \right) & \end{aligned} \quad (2.3)$$

Before proceeding to give physical meaning to the system (Eq. (2.3)), we reformulate it by replacing the fluctuating density ρ' by the fluctuating pressure p' which is the more natural acoustic variable, (see ref. 4). We assume that the flow is isentropic and has no mean temperature gradient. It then follows that

$$p = A \rho^\gamma$$

or

$$\rho' = \frac{p'}{c_0^2} + O(p'^2) = \frac{p'}{c_0^2} + q \quad (2.5)$$

where c_0 is the ambient speed of sound (constant under the above assumptions) and q is some quadratic term. We can then replace ρ' in (2.3) by p' and get

$$\begin{aligned} \frac{1}{c_0^2} \frac{\partial p'}{\partial t} + \frac{1}{c_0^2} \text{div}(p' \vec{U}) + \text{div}(\bar{\rho} u') &= -\text{div}(\bar{\rho} \vec{U} + \rho' u' + q \vec{U}) - \frac{\partial q}{\partial t} ; \\ \bar{\rho} \left(\frac{\partial u_i'}{\partial t} + \bar{U}_j \frac{\partial u_i'}{\partial y_j} + u_j' \frac{\partial \bar{U}_i}{\partial y_j} \right) + \frac{p'}{c_0^2} \bar{U}_j \frac{\partial \bar{U}_i}{\partial y_j} + \frac{\partial p'}{\partial y_j} &= \\ \frac{\partial e_{ij}}{\partial y_j} - \frac{\partial \bar{p}}{\partial y_j} - \left[\bar{\rho} \bar{U}_j \frac{\partial \bar{U}_i}{\partial y_j} - \rho u_j \frac{\partial u_i'}{\partial y_j} \right] - q \bar{U}_j \frac{\partial \bar{U}_i}{\partial y_j} &= \\ -\rho' \left[\bar{U}_j \frac{\partial u_i'}{\partial y_j} + u_j' \frac{\partial \bar{U}_i}{\partial y_j} + \frac{\partial u_i'}{\partial t} \right] & \end{aligned}$$

The system (2.6) has on the left hand side all of the first order interacting terms between the fluctuating and mean quantities (provided q as given in (2.5) is quadratic, which will be the case if the jet is isentropic). The terms on the right hand side are considered as the source terms and are all of higher order. (Not all of these terms are of equal importance in the generation of sound, see reference 5.)

In this study, it is assumed that an artificial source is injected into the jet and that the magnitude of this source is much larger than the real sources in the jet. Therefore, the system (2.6) will become the following inhomogeneous linear system

$$\frac{1}{c_0^2} \frac{\partial p'}{\partial t} + \frac{1}{c_0^2} \text{div}(p' \vec{U}) + \text{div}(\bar{\rho} u') = f_1(t, x, y, z) \quad (2.7)$$

$$\bar{\rho} \left(\frac{\partial u_i'}{\partial t} + \bar{U}_j \frac{\partial u_i'}{\partial y_j} + u_j' \frac{\partial \bar{U}_i}{\partial y_j} \right) + \frac{p'}{c_0^2} \bar{U}_j \frac{\partial \bar{U}_i}{\partial y_j} + \frac{\partial p'}{\partial y_j} = g_i(t, x, y, z)$$

For this study, the forcing terms will be chosen as

$$f(t, x, y, z) = f(t) \delta(|\vec{x} - \vec{x}_0|)$$

$$g_i(t, x, y, z) = 0$$

where \vec{x}_0 is a given axial point downstream of the jet exit. The function $f(t)$ is chosen to give rise to a pulse-like solution and has the form

$$f(t) = e^{-(at^2 + \frac{b}{t^2})} \quad t \geq 0$$

for suitable (positive) constants a and b . The δ -function is modelled by a Gaussian. This source corresponds to a monopole source if there is no flow. As mentioned previously, it is not the intention to model the real sources in the jet, but rather to study the interaction between an acoustic source and the mean flow.

The system (2.7) is a linear first order hyperbolic system which includes all of the first order terms for the fluctuating field in response to the given input forcing term. The fluctuating quantities will have an irrotational component in the near field (see refs. 23 and 24) where the mean square

velocity decays inversely with the fourth power of the distance. Farther from the source, the mean square fluctuating velocity will decay with the second power of the distance thus reducing to a purely acoustic field.

If a parallel transverse mean flow is assumed, then (2.7) can be reduced to the third order Lilley equation. This is not efficient for a full numerical solution. In this work, we will use a realistic jet velocity profile of an axially symmetric spreading jet obtained by Maestrello (ref. 24). Assuming an axially symmetric source on the right hand side, the fluctuating solution to (2.7) will also be axially symmetric and thus the system (2.7) can be reduced to a system for three dependent variables, the fluctuating pressure p' , and the fluctuating axial and normal velocities u' and v' .

It is clear from the system (2.7) that in order to correctly simulate a real jet, both the type and the location of the sources for a given mean flow are important (as pointed out in ref. 11). In the present paper, we will study the phenomena of interaction for a fixed type of source, and the dependence of this interaction on the location and the mean velocity.

III. NUMERICAL SCHEME

In this section, we discuss the numerical scheme used to solve (2.7). We will use z and r as cylindrical coordinates along the axis of the jet and normal to the jet respectively. A typical computational domain is shown in figure 1. In this figure, the computations are conducted in the piecewise rectangular region downstream of the nozzle boundary and bounded by the far-field boundary. The solution is extremely sensitive to the far-field boundary conditions and these as well as the boundary conditions at the nozzle boundary will be discussed in the next section. Note that the shear layer is not a

boundary. The mean profile of Maestrello models the shear layer as a continuous function (see ref. 24). Coordinate stretching is used to increase the resolution in the vicinity of the shear layer and the sources.

To describe the numerical scheme, we will rewrite the system (2.7) in simpler form assuming

$$p_0 = p_\infty = \text{constant} \quad (3.1)$$

The assumption (3.1) is reasonable as far as investigating the interaction phenomena. With this assumption, and dropping the primes and the bars for simplicity, we obtain the following linear first order system (in normalized coordinates so that $c_0^2 = 1$).

$$\begin{aligned} p_t + (U_0 p + u)_z + (V_0 p + v)_r + \frac{V_0 p + v}{r} &= f ; \\ u_t + (U_0 u + p)_z + (V_0 u)_r &= uV_{0,r} - vU_{0,r} ; \\ v_t + (U_0 v)_z + (V_0 v + p)_r &= vU_{0,z} - uV_{0,z} ; \end{aligned} \quad (3.2)$$

where U_0 and V_0 are the mean axial and radial velocities respectively, and the subscripts denote differentiation. The solution is assumed to start from a state of rest i.e., $p, u, v = 0$ at $t = 0$. The above system can be written in the following symbolic form

$$w_t + F_z + G_r = H \quad (3.3)$$

where w is the vector (p, u, v) and F, G, H are explicit functions which can be obtained from (3.2).

To advance the solution from time t to $t + 2\Delta t$, we use the method of time splitting (ref. 25). Thus, if $L_z(\Delta t)$ and $L_r(\Delta t)$ denote symbolic solution operators to the one-dimensional equations

$$\begin{aligned} w_t^1 + F_z &= H_1 \\ w_t^2 + G_r &= H_2 \end{aligned} \quad (3.4)$$

then the solution to (3.3) is advanced by the formula

$$w(t + 2\Delta t) = L_z(\Delta t)L_r(\Delta t)L_r(\Delta t)L_z(\Delta t)w(t) \quad (3.5)$$

This procedure is second order accurate in time. (i.e., the truncation error in (3.4) is $O(t^3)$.)

Using the method of splitting, one can employ spatial discretizations solving only one-dimensional systems. In this study, it was soon realized that a high order accurate scheme was essential to resolve the solution up to the far field. We, thus, use a scheme developed by Gottlieb and Turkel (ref. 26), which is fourth order accurate in the spatial variables. For the one-dimensional equations in (3.4), we have

$$\bar{w}_i(t + \Delta t) = w_i(t) + \frac{\Delta t}{6\Delta x} (7F_i - 8F_{i+1} + F_{i+2}) + \Delta t H_i \quad (3.6)$$

$$w_i(t + \Delta t) = \frac{1}{2}(w_i(t) + \bar{w}_i(t + \Delta t)) + \frac{\Delta t}{6} (7\bar{F}_i + 8\bar{F}_{i-1} - \bar{F}_{i-2}) + \Delta t \bar{H}_i$$

here \bar{F}_i denotes F evaluated at \bar{w}_i etc. Further details can be found in reference 26. The scheme based on (3.6) can be implemented on the CDC STAR-100 with great efficiencies.

Since the solution is required at many jet diameters (~ 50), large numbers of grid points are required for accuracy. This restricts the

applicability of the method to cases where the wave length is of the order of the nozzle diameter. If only time harmonic solutions are of interest, the solution of the time dependent equations can be regarded as a relaxation scheme to obtain the time harmonic solution. In this case convergence is achieved by integrating until the transient has passed out of the computational domain. A solution of the time harmonic problem by direct methods is not possible because of the large number of unknowns involved. Assuming a single wave solution of the form

$$A(\vec{x})e^{ikS(\vec{x})}$$

for slowly varying real quantities A and S , as done in references 21 and 22 is not feasible, since multiple waves can be expected to be present due to interaction with the shear layer.

IV. BOUNDARY CONDITIONS

Our experience has indicated that the most important feature in obtaining accurate solutions is correct specification of the boundary conditions. We point out that the problem is posed in the spatially infinite region without the far-field and nozzle boundaries in Figure 1. These artificial boundaries are necessary only for the purposes of numerical computation. Care must be exercised to prevent false reflections generated at the boundaries from moving in and destroying the solution.

As indicated in the figure, two types of artificial boundaries are present. The far-field radiation boundary where an approximation to outgoing waves must be specified and the nozzle boundary where one must stipulate that no acoustic energy flows down the pipe into the computational domain.

We first deal with the far-field radiation boundaries. It is clear that if U_0 vanishes in say (3.2), p will satisfy the wave equation. Spherical outgoing waves have the form (if c_0 is normalized to unity).

$$p(t,d) = f(t - d)/d \quad (4.1)$$

where $d = |\vec{x}|$ and \vec{x} denotes the spatial position. The formula (4.1) was extended to general solutions of the wave equation by Friedlander (ref. 27) who proved that under certain conditions p would have a convergent expansion of the form

$$p(t,d) = \sum_{j=1}^{\infty} f_j(t - d, \theta)/d^j \quad (4.2)$$

where θ is the polar angle (axial symmetry is assumed). Less restrictive conditions under which (4.2) is valid as an asymptotic expansion are given by Bayliss and Turkel (ref. 28).

In order to derive boundary conditions to match the solution to (4.2), we introduce the operator

$$L = \frac{\partial}{\partial t} + \frac{\partial}{\partial d} \quad (4.3)$$

and point out that, in the case of harmonic time dependence, the operator (4.3) reduces to

$$-ik + \frac{\partial}{\partial d}$$

Then, the statement

$$Lp \rightarrow 0 \quad (d \rightarrow \infty)$$

is exactly the Sommerfeld radiation condition. However, at a finite d , the relation

$$Lp = 0$$

is not exact even for the first term in the expansion (4.2) (or for a spherical wave (4.1)). If, however, (4.3) is modified by introducing

$$B_1 = L + \frac{1}{d}$$

then it is easy to verify that

$$B_1 p = 0 \tag{4.4}$$

is exact for the first term in (4.2) or for (4.1). This is, therefore, the appropriate, finite form of the Sommerfeld radiation condition.

In general (4.4) will not be accurate if the boundary is close in and if the sources are not monopoles. To obtain accurate boundary conditions in these cases, we extend the operator B_1 to annihilate more terms in the expansion (4.2). In fact, introducing the operator

$$B_m = \prod_{j=1}^m \left(L + \frac{2j-1}{d} \right)$$

it can be easily verified that B_m annihilates exactly the first m terms in the expansion (4.2).

It can also be shown (ref. 27) that the boundary conditions

$$B_m p = 0$$

give rise to well posed problems in the cylindrical space of Figure 1. The second order operator has been applied to the study of several sources in a

jet and quadrupole sources where (4.4) is not sufficiently accurate. For most of the work reported in this paper, it has been verified by computing the solution with different boundaries and comparing the solution at fixed interior points that (4.4) is sufficient. It has also been verified that direct application of the Sommerfeld condition is very inaccurate.

It is finally pointed out that, since the fluctuating velocities are dependent variables, it is possible to use (2.5) (with $U_0 = 0$ in the far field) to solve

$$\frac{\partial p}{\partial d} = - \frac{\partial \tilde{u}}{\partial t}$$

where \tilde{u} is the radial velocity. Thus, B can be replaced by the operator

$$\frac{\partial p}{\partial t} - \frac{\partial \tilde{u}}{\partial t} + \frac{p}{d} = 0$$

which can be implemented without spatial differences.

We next consider appropriate boundary conditions in the nozzle. Physically it is intended to simulate a semi-infinite pipe of constant diameter. This is a reasonable assumption since the numerical sources are located in the jet. The boundary condition must simulate that no acoustic information travels down the pipe into free space. We assume that, in the pipe, the mean flow, U_0 , is constant and is purely axial. We will also work with nondimensional coordinates and will, therefore, denote the mean flow by M , where M is the exit Mach number of the jet. The system (2.5) then becomes

$$\frac{\partial p}{\partial t} + M \frac{\partial p}{\partial z} + \frac{\partial u}{\partial z} + \frac{\partial v}{\partial r} + \frac{v}{r} = 0 \quad (a)$$

$$\frac{\partial u}{\partial t} + M \frac{\partial u}{\partial z} + \frac{\partial p}{\partial z} = 0 \quad (b) \quad (4.5)$$

$$\frac{\partial v}{\partial t} + M \frac{\partial v}{\partial z} + \frac{\partial p}{\partial r} = 0 \quad (c)$$

The system (4.5) can be reduced to a convective wave equation for p ,

$$\frac{\partial^2 p}{\partial t^2} + 2M \frac{\partial^2 p}{\partial z^2} + M^2 \frac{\partial p}{\partial z} - \Delta p = 0 \quad (4.5d)$$

where $\Delta = \nabla \cdot \nabla$. If the pipe has normalized diameter 1, then the boundary conditions for p are

$$\frac{\partial p}{\partial r} = 0 \quad (r = \frac{1}{2}) \quad (a) \quad (4.6)$$

$$\frac{\partial p}{\partial r} = 0 \quad (r = 0) \quad (b)$$

The condition (4.6a) is equivalent to the condition $v = 0$ on the pipe wall, while (4.6b) is a consequence of axial symmetry.

We now look for solutions to (4.5d) with the dependence

$$p = e^{ikt} e^{i\ell z} h(r) \hat{p} \quad (4.7)$$

where k , the nondimensionalized frequency, is taken as positive. The condition for modes to propagate up the pipe is

$$\text{Real Part } \ell > 0 \quad (4.8)$$

Upon substituting (4.7) into (4.5d), we obtain an equation for h ,

$$\frac{1}{r}(rh')' + \lambda h = 0 \quad (4.9)$$

where

$$\lambda = k^2 + 2\ell kM - \ell^2(1 - M^2) \quad (4.10)$$

The solution to (4.9) satisfying (4.6b) is

$$h(r) = J_0(\lambda^{1/2}r)$$

and thus the values of λ are restricted to a discrete set $\{\lambda_n\}$, such that $\lambda_n^{1/2}$ is twice the n^{th} zero of J_0' . Solving (4.11) for ℓ results in the formula

$$\ell_n = \frac{kM \pm \sqrt{k^2M^2 + (k^2 - \lambda_n)(1 - M^2)}}{(1 - M^2)} \quad (4.11)$$

Thus, for any k , there are only a discrete set of modes present in the duct, with longitudinal wave numbers given by (4.11).

If $n = 0$, $\lambda_n = 0$, (4.11) yields

$$\ell = \frac{k}{1 - M} \quad (a) \quad (4.12)$$

$$\ell = \frac{-k}{1 + M} \quad (b)$$

and (4.8) implies that only (4.12a) corresponds to a mode traveling up the pipe. For $n > 0$, ℓ will not be real for sufficiently small k . In fact, this will be so provided

$$k \leq \sqrt{\lambda_1} \sqrt{1 - M^2} \quad (4.13)$$

and $\sqrt{\lambda_1} \leq 7.66$ (twice the first zero of J_0'). For these values of k , the

upstream propagating modes will decay exponentially as the distance up the pipe increases. It then follows that upstream of the nozzle, if k is restricted by (4.13), the mode given by (4.12a) will describe the upstream propagating solution.

It only remains to describe the velocities associated with (4.12a) so that appropriate boundary conditions can be obtained. It follows from $\lambda_0 = 0$ and (4.5c) that $v = 0$. Upon setting

$$u = e^{ikt} e^{ilz} h(r) \hat{u}$$

and substituting into (4.5b) (making use of (4.7)), we obtain

$$ik\hat{u} + M il\hat{u} + il\hat{p} = 0$$

and from (4.12b) we obtain

$$\hat{u} + \hat{p} = 0 ,$$

i.e. $u + p = 0$. The resulting boundary conditions in the nozzle are thus

$$\begin{aligned} u + p &= 0 & (a) \\ v &= 0 & (b) \end{aligned} \tag{4.14}$$

The boundary conditions (4.14) are generally applied at the same distance upstream as the far-field boundary. Of course, in principle the problem of the nozzle boundary can be avoided by taking the nozzle boundary sufficiently far upstream so that no spurious reflection can occur during the time that it takes for the pulse to pass through the computational domain. This, however, would severely complicate the program. In practice extensive numerical experiments have revealed virtually no effect on the far-field solution by applying

the conditions (4.14) at any distance upstream of the exit pipe. This is probably due to the exponential decay of the higher modes and the fact that very little energy propagates upstream of the nozzle exit.

V. EXPERIMENT

Measurements of the time dependent pressure in the far field were made inside an anechoic chamber about an arc of 5.79 m from the source. The source consisted of a 1.0 cm diameter tube exiting from the center of a standard convergent type nozzle with diameter $D = 5.08$ cm. The tube extends downstream $1.25D$ from the nozzle exit. Upstream, the tube extends into the settling chamber, diverges and exits through the settling chamber to the outside. The mean flow profile and the experimental configuration are shown in figure 2. The profile has a virtual origin (z_0) at $2.57 D$ upstream of the nozzle exit and a spread of nearly 11° . In the figure, U_j denotes the jet exit velocity. The static pressure shown in the figure has not been included in the numerical calculations at the present time. Further details can be found in reference 24.

Two types of sources were studied. A pure tone was generated by using an acoustic driver at the end of the tube. A pulse was generated by using a conventional shock tube type of chamber with a diaphragm. The pulse is created by breaking the diaphragm. The pressure across the diaphragm exceeds 100 psi (6.3×10^5 pascal).

Because of this high pressure, the amplitude from the pulse was greater than the noise produced by the jet flow for the conditions tested by 30 dB. The high pressure of the pulse also insured that the power output from the source was unaffected by the presence of the flow. It was not possible to generate a pure tone with output unaffected by the flow and thus only the pulse will be considered further.

The temperature in the jet was ambient and tests were conducted at exit Mach numbers ranging from 0.33 to 1.2. Two different sizes of condenser type microphones were used independently. Their diameters were 1.25 cm and 0.63 cm. The microphones were verified to have a flat response in the range of frequencies considered. Only the data obtained by the 1.25 cm microphones are considered, because no difference in either frequency response or amplitude level was found between the two different size microphones.

The microphones were placed at 10° intervals between 10° and 130° from the direction of flow. The acoustic pressure was recorded on an FM magnetic tape recorder in the range 25 Hz to 40 kHz although the data presented in this paper only cover the range 200 Hz to 15 kHz. Data reduction was accomplished using both analog and digital means.

VI. RESULTS AND DISCUSSION

Experimental and numerical results are presented for the far-field acoustic pressure. These results include:

- a) The real time pressure pulse with and without flow,
- b) The intensity as a function of the angle θ for a range of Strouhal numbers. ($St = \frac{fD}{U_j}$ where f is the frequency and D the jet diameter),
- c) The acoustic power integrated over a large far-field sphere as a function of Strouhal number,
- d) The acoustic power integrated over a large far-field sphere as a function of Strouhal number based on the source position for different source location.

Figures 3a through 6b show the nondimensional far-field time dependent pulse $p(t)$, with and without the flow through the nozzle, for both the experiment and the numerical simulation. Figures 3a and 3b show the

experimental results for θ (measured from the jet axis) between 10° and 130° with no flow. It is clear from the figure that the experimental source is not omni-directional. In fact, the peak output occurs near the jet axis and decreases nearly uniformly as the angle θ increases. It is known (ref. 29) that, at low pressure, the output from the tube is omni-directional (at least for low frequencies). However, at such high pressures, the experimental source is not a monopole.

Figures 4a and 4b show the equivalent pulse with the flow at an exit Mach number of 0.66. The effect of refraction of sound through the shear layer is clearly noticeable by the stretching out of the pressure field and by the decay in amplitude at low angles from the axis of the jet. At mid angles (i.e. $\theta \approx 30^\circ$), both positive and negative peaks well exceed the amplitude of the no flow case indicating a low frequency amplification, a phenomena not totally accountable by classical refraction theory. The high frequency oscillations after the main peaks are also strongly reduced.

Figures 5a and 5b show the numerical counterpart with no flow for angles from 0° to 170° . As can be seen, the input source is nearly omni-directional and thus can be considered a monopole source. The experimental source on the other hand, contains both a mass and a force fluctuation as can be seen in figure 3. At present, the numerical simulation has only been run with monopole sources, since the monopole will exhibit qualitative agreement with the experiment. The time duration of the numerical pulse is nearly twice as long as the duration of the experimental pulse. This was necessary because of numerical difficulties in computing narrower pulses at large distances from the source.

Figures 6a and 6b show the equivalent pulse with flow (exit Mach number .66). As with the experimental pulse, the effect of refraction is noticeable

by a severe stretching out of the pulse accompanied by a decay in amplitude at low angles from the jet axis. It is also clear that an increase in amplitude, similar to that measured in the experiment, occurs at mid angles. An additional feature of the numerical pulse is the occurrence of a low frequency oscillation behind the main peak of the pulse. This is present only in the mid angle range where the amplification occurs.

The previous figures indicate the possibility of amplification of sound in the presence of flow. In order to quantify the amplification or attenuation of the sound due to the flow, a comparison is made of the power ratio with and without flow. The power output is computed around a large sphere surrounding the source. However, a small amount of acoustic energy propagates upstream through the nozzle. This additional energy flux through the nozzle is computed by the following formula (ref. 30):

$$I = \frac{1}{\rho_0} (p' + \rho_0 u' \cdot U_0)(\rho_0 u' + \rho' U_0) \quad (6.1)$$

which is the acoustic intensity in the presence of an irrotational mean flow. Here, the primed quantities denote the acoustic perturbation while U_0 and ρ_0 denote the mean velocity and density. The energy flux through the nozzle is computed upstream of the nozzle exit as indicated in figure 1.

At the upstream nozzle boundary, we use (4.4) with (6.1) to obtain the following total intensity (using nondimensionalized coordinates)

$$I_T = \int_{-\infty}^{\infty} dt (1 - M)^2 p^2 \quad (6.2)$$

An experimental attempt was made to measure the acoustic power due to the pulse upstream of the nozzle, using two microphones inside the settling

chamber. The output from the microphones, during and immediately after the burst, showed an insignificant increase in level from the background. This indicated that very little sound is propagated upstream. The numerical computation of the power upstream through the nozzle also showed that this was always much less than 5 percent of the total acoustic power.

In the far field (6.1), together with the boundary conditions discussed previously, yields the well known result (again using nondimensional coordinates)

$$I_T = \int_{-\infty}^{\infty} p^2(t) dt \quad (6.2)$$

for the total intensity at a point on the far field arc. In the frequency domain, the intensity per unit frequency at an angle θ is

$$I(\theta, \omega) = |\hat{p}(\omega)|^2$$

where $\hat{p}(\omega)$ is the Fourier transform of the pressure pulse.

Figures 7a and 7b show the experimental acoustic intensity ratio $I(\theta, f)_{\text{flow}} / I(\theta, f)_{\text{no flow}}$ (where $\omega = 2\pi f$) for various Strouhal numbers, as a function of the far-field angle θ . The figures show that the maximum amplification occurs at about 30° from the jet axis for all of the frequencies plotted. For some of the frequencies, there is also an amplification at 130° . There is, however, very little energy present at large angles and thus this does not affect the total acoustic power. It is noted that the angle of maximum intensity is relatively insensitive to frequency, a feature that would not be expected from classical refraction theory.

Figure 7c shows the numerical counterpart of the previous figures. The peak amplification now occurs at about 40° because the numerical pulse

is omni-directional. Since the numerical computation is restricted to a broader pulse, the numerical results are limited to the low frequency part of the spectrum. In this range of frequencies, the numerical and experimental results are qualitatively consistent.

Figures 8a and 8b show the power ratio $W(f)_{\text{flow}}/W(f)_{\text{no flow}}$ for both the experiment and the numerical simulation, as a function of both Strouhal number based on jet diameter (fd/u_j) and Strouhal number based on the distance of the sources (z) from the nozzle exit (fz/u_j). The evaluation of the experimental acoustic power is limited to an arc between 0° and 130° from the direction of flow. The experimental pulse is very weak for angles approaching 130° (see figs. 3a, b and 4a, b) and thus the higher angles would make a negligible contribution to the total power. The numerical computation of the power includes all angles up to 170° at 10° intervals as well as the power propagating upstream of the nozzle. There is virtually no difference in the power ratio, when it is summed at 5° intervals.

The experimental curve shows amplification up to $fd/U_j = 1.2$ with a maximum at $fd/U_j = .4$. In addition, there is a reduction for fd/U_j greater than 1.5. The numerical curve shows an increase in power for fd/U_j between .15 to .3 with a peak at $fd/U_j = .21$ which appears to be independent of the jet velocity. Since the numerical simulation cannot, at present, accurately compute higher frequencies, the power reduction at higher Strouhal numbers cannot be verified. It is believed that turbulent scattering will have some contribution to this reduction. The numerical results also show an increase in power ratio for fd/U_j of the order 0.1. This cannot be shown experimentally because the far-field measurements would have to be taken at several hundred diameters to account for the low frequencies and also because the anechoic

chamber is not an effective absorber at these frequencies. This effect, however, can be seen in the experiment by observing the stretching of the real time pulse with flow (see fig. 4a). The total power in this frequency range is very small for both the experimental and numerical pulse.

The power ratio curves are sensitive to the pulse width and the distance of the source from the jet exit. However, when the power ratio is plotted in terms of Strouhal number based on the distance of the source from the jet exit (fz/U_j) it is found that the maximum occurs at a Strouhal number nearly independent of source position. This can be seen in figure 9 where the power ratio is shown for numerical simulations at four different source positions.

The behavior of this far-field amplification is very similar to the growth rate of instability waves in an unexcited jet. Such behavior has been verified both experimentally and analytically (refs. 16 and 19). The results in figure 9 indicate that virtually no amplification occurs if the source is well downstream of the potential core, where instability waves are known to be insignificant (see ref. 19). This is clear evidence that amplification will occur only if the source is within or just after the potential flow core of the jet where instability waves can be sustained. In addition, the maximum amplification occurs at roughly 3 diameters downstream of the nozzle, which is consistent with the experimental measurements in reference 19.

The present experimental results (fig. 8a) show a maximum amplification rate at fz/U_j of about .6, which is roughly twice the position of the numerical peak. This may be due to the fact that the numerical pulse is nearly twice as broad as the experimental pulse, or to the fact that the numerical pulse is omni-directional.

The results presented here support the hypothesis that an acoustic source placed within the potential core of the jet excites instability waves, the

result of which is an amplification of the far-field sound. This is also consistent with the experiments of Moore (ref. 16) and Bechert and Pfizenmaier (ref. 17) where an increase in broadband power was observed by acoustically exciting the jet upstream of the nozzle.

The strong amplification at the mid-angles and at frequencies of maximum power ratio is due to the terms involving the interaction of the acoustic velocities with the gradient of the mean flow (see (3.2)). If one omits these terms, a directivity pattern is obtained which increases monotonically with the angle from the flow, similar to the patterns obtained in references 20 and 21. This indicates that these terms are very important in producing the power amplification.

The variation in total acoustic power with Mach number $(T(M)_{\text{flow}}/T(M)_{\text{no flow}})$ for both the experimental and numerical pulses is shown in figure 10. The experimental power increases with increasing Mach number and rises rapidly beyond a Mach number of 0.5. This figure will change with the shape of the pulse and the source position but the qualitative features will be similar.

The experimental results exhibit a larger total amplification than the numerical simulation. A possible reason is the lack of nonlinear effects in the numerical scheme. The experiment also contains interaction between the acoustic and turbulent fields which is not present in the numerical calculations and which is known as a cause of attenuation at high frequencies. It is clear, however, that the experimental and numerical results are qualitatively consistent.

VII. CONCLUSION

An amplification of total power output is observed when a source is located within the potential flow core of a jet. This amplification occurs in the

range of frequencies where the local instability waves have the strongest growth rate. The acoustic power amplification exhibits a peak which is similar to that which is observed both experimentally and analytically for instability waves in an unexcited jet. This is particularly true when the amplification rate is plotted as a function of Strouhal number based on the distance of the source from the nozzle. These results show that instability waves can act as a mechanism to amplify the sound from an acoustic source. Further evidence is found in the fact that no peak occurs if the source is far downstream of the potential flow core. The quantitative differences between the numerical simulation and the experiment are probably associated with nonlinear terms, the presence of turbulence, and possibly the different source structures. For higher frequencies, a reduction in sound is experimentally observed. This result suggests that modification of the stability characteristics of the jet, together with the observed attenuation at higher frequencies, may be viable mechanisms for the suppression of sound.

REFERENCES

1. Lighthill, M. J.: On Sound Generated Aerodynamically - I. General Theory. Proceedings of the Royal Society A211, pp. 564-578, 1952.
2. Lighthill, M. J.: On Sound Generated Aerodynamically - II. Proceedings of the Royal Society A222, pp. 1-32, 1954.
3. Phillips, O. M.: On the Generation of Sound By Supersonic Turbulent Shear Layers. Journal of Fluid Mechanics, Vol. 9, pp. 1-28, 1960.
4. Doak, P. E.: Fundamentals of Aerodynamic Sound Theory and Flow Duct Acoustics. Journal of Sound and Vibration, Vol 28, pp. 527-561, 1973.
5. Lilley, G. M.: Theory of Turbulence Generated Jet Noise: Generation of Sound In A Mixing Region. United States Air Force Technical Report AFAPL-TR-72-53, Vol. IV, 1972.
6. Tester, B. J. and Morfey: Developments in Jet Noise Modelling - Theoretical Predictions and Comparison with Measured Data. Journal of Sound and Vibration, Vol. 46, pp. 79-103, 1976.
7. Mungur, P., Plumblee, H. E., and Doak, P. E.: Analysis of Acoustic Radiation In A Jet Flow Environment. Journal of Sound and Vibration, Vol. 36, pp. 21-52, 1974.
8. Miles, J. W.: On the Reflection of Sound at the Interface of Relative Motion. Journal of the Acoustical Society of America, Vol. 29, 1957.
9. Ribner, H. S.: Reflection, Transmission and Amplification of Sound by a Moving Medium. Journal of the Acoustical Society of America, Vol. 29, pp. 435-441, 1957.
10. Mani, R.: The Influence of Jet Flow On Jet Noise. Part 1. The Noise of Unheated Jets. Journal of Fluid Mechanics, Vol. 73, Pt. 4, pp. 753-778, 1976.
11. Dowling, A. P., Ffowcs Williams, J. E., and Goldstein, M. E.: Sound Production in A Moving Stream. Philosophical Transactions of The Royal Society of London, Vol. 288, No. 1353, pp. 321-349, 1978.
12. Howe, M. S.: Transmission of An Acoustic Pulse Through A Plane Vortex Sheet. Journal of Fluid Mechanics, Vol. 43, Pt. 2, pp. 353-367, 1970.
13. Morris, P. J. and Tam, C. K. W.: Near and Far-Field Noise from Large-Scale Instabilities of Axisymmetric Jets. AIAA 4th Aeroacoustics Conference, Paper Number 77-1351, 1977.
14. Vlasov, Ye. V. and Ginevskiy, A. S.: Generation and Suppression of Turbulence In an Axisymmetric Turbulent Jet in the Presence of An Acoustic Influence. NASA TT-F15, 721, 1974.

15. Tam, C. K. W.: Excitation of Instability Waves in A Two-Dimensional Shear Layer by Sound. *Journal of Fluid Mechanics*, Vol. 89, pp. 357-371, 1978.
16. Moore, C. J.: The Role of Shear-Layer Instability Waves In Jet Exhaust Noise. *Journal of Fluid Mechanics*, Vol. 80, Pt. 2, pp. 321-367, 1974.
17. Bechert, D. and Pfizenmaier, E.: On The Amplification of Broadband Jet Noise By Pure Tone Excitation. *Journal of Sound and Vibration*, Vol. 43, pp. 581-587, 1975.
18. Kibens, V.: Discrete Noise Spectrum Generated by an Acoustically Excited Jet. AIAA 5th Aeroacoustics Conference, Paper Np. 79-0592, 1979.
19. Maestrello, L. and Fung, Y. T.: Quasi-Periodic Structure of a Turbulent Jet. *Journal of Sound and Vibration*, Vol. 64, pp. 107-122, 1979.
20. Mattingly, G. E. and Chan, C. C.: Unstable Waves On an Axisymmetric Jet Column. *Journal of Fluid Mechanics*, Vol. 65, Pt. 3, pp. 54;-560, 1974.
21. Schubert, L. K.: Numerical Study of Sound Refraction by a Jet Flow. II. Wave Acoustics. *Journal of the Acoustical Society of America*, Vol. 51, pp. 439-446, 1972.
22. Liu, C. H. and Maestrello, L.: Propagation of Sound Through a Real Jet Flow Field. *AIAA Journal*, Vol. 13, pp. 66-70, 1975.
23. Phillips, O. M.: The Irrotational Motion Motion Outside the Free Turbulent Boundary. *Proceedings of the Cambridge Philosophical Society*, Vol. 51, pp. 222-229, 1955.
24. Maestrello, L.: Acoustic Energy Flow from Subsonic Jets and Their Mean and Turbulent Flow Structure. Ph.D Thesis, Institute of Sound and Vibration. 1975.
25. Strang, W. G.: On The Contruction and Comparison of Difference Schemes. *SIAM Journal of Numerical Analysis*, Vol. 5, pp. 506-517, 1968.
26. Gottlieb, D. and Turkel, E.: Dissipative Two-Four Methods for Time-Dependent Problems. *Mathematics of Computation*, Vol. 30, pp. 703-723, 1976.
27. Friedlander, F. G.: On The Radiation Field of Pulse Solutions of the Wave Equation. *Proceedings of the Royal Society A*, Vol. 269, pp. 53-65, 1962.
28. Bayliss, A. and Turkel, E.: Radiation Conditions for Wavelike Equations. ICASE Report 79-26. 1979.
29. Grande, E.: Refraction of Sound by Jet Flow and Jet Temperature II. Institute for Aerospace Studies, University of Toronto, NASA CR 840, 1967.
30. Goldstein, M. E.: Aeroacoustics. McGraw Hill, NY, pp. 41-42, 1976.

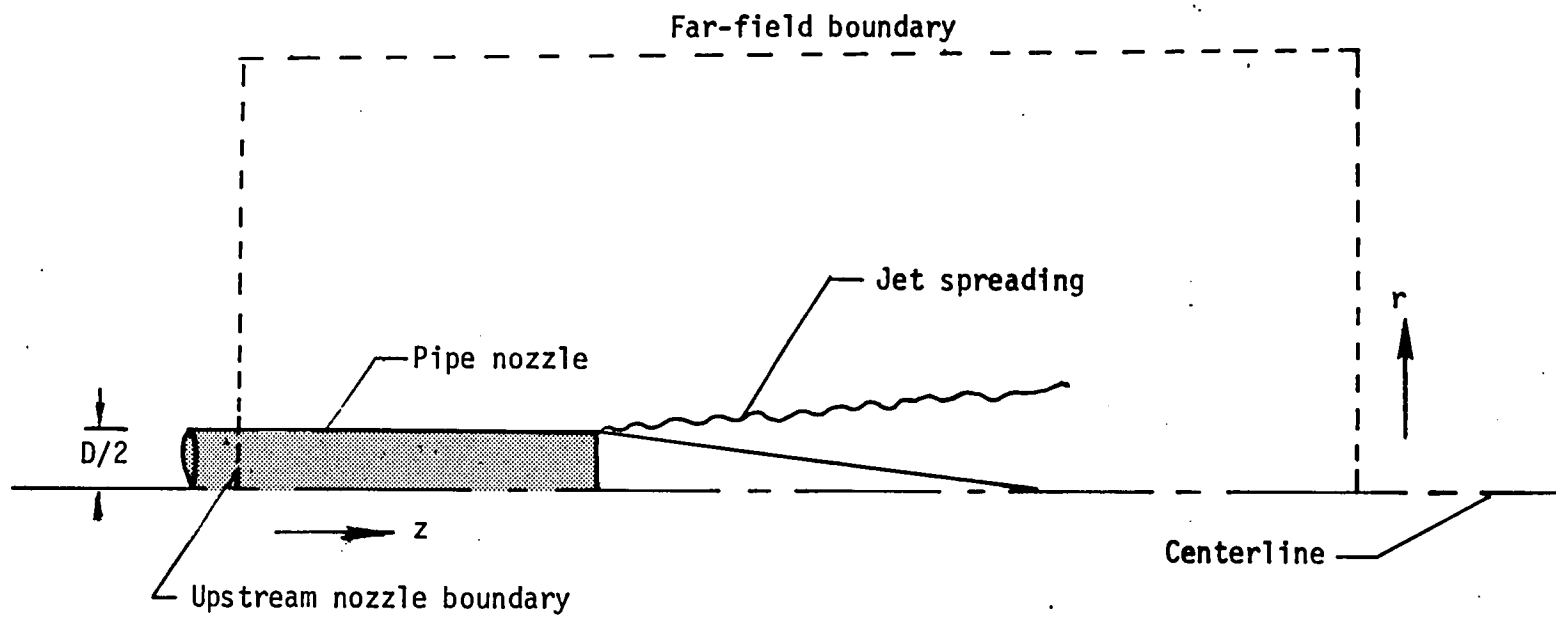


Figure 1. Computational domain

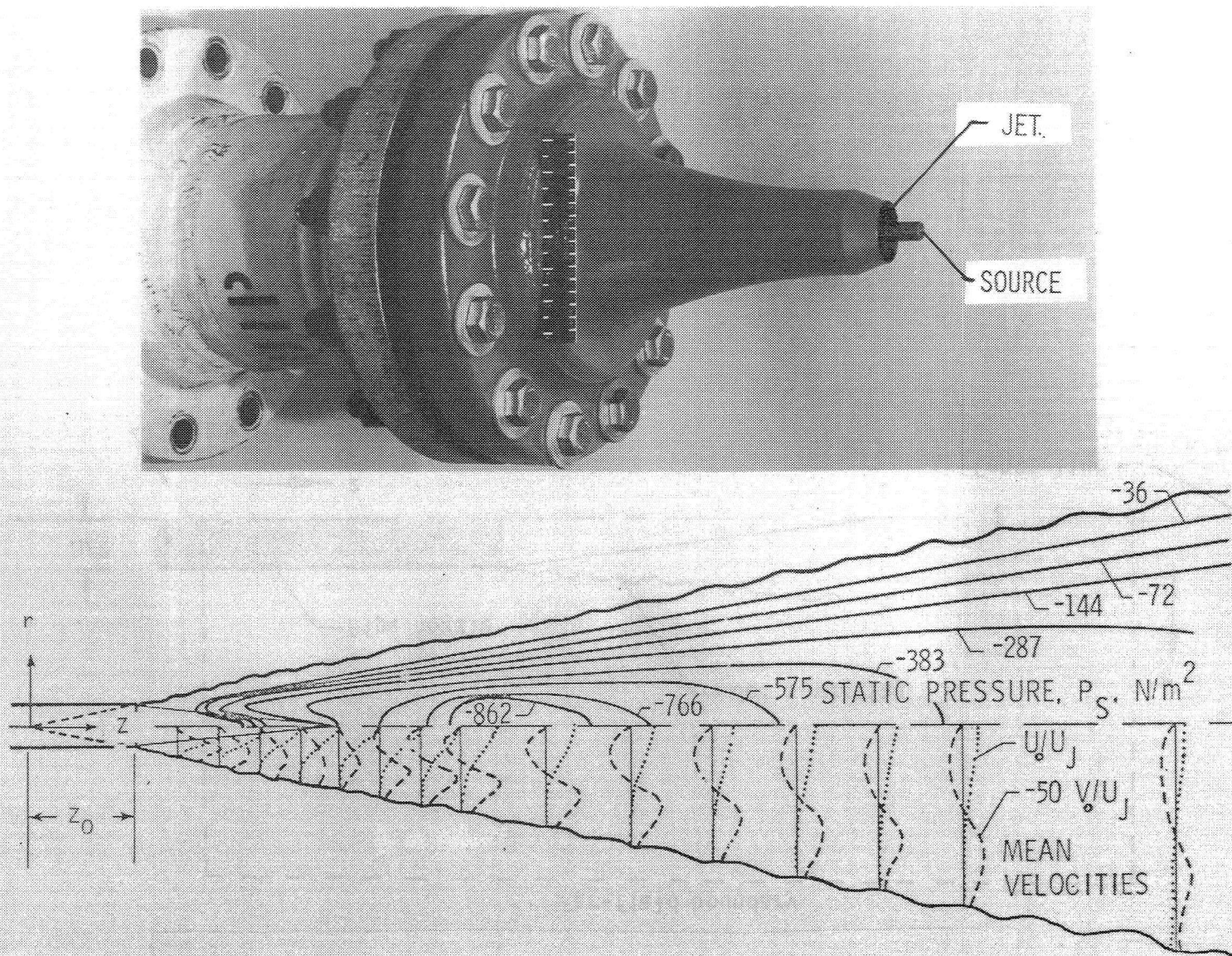


Figure 2. Experimental configuration and mean flow field.

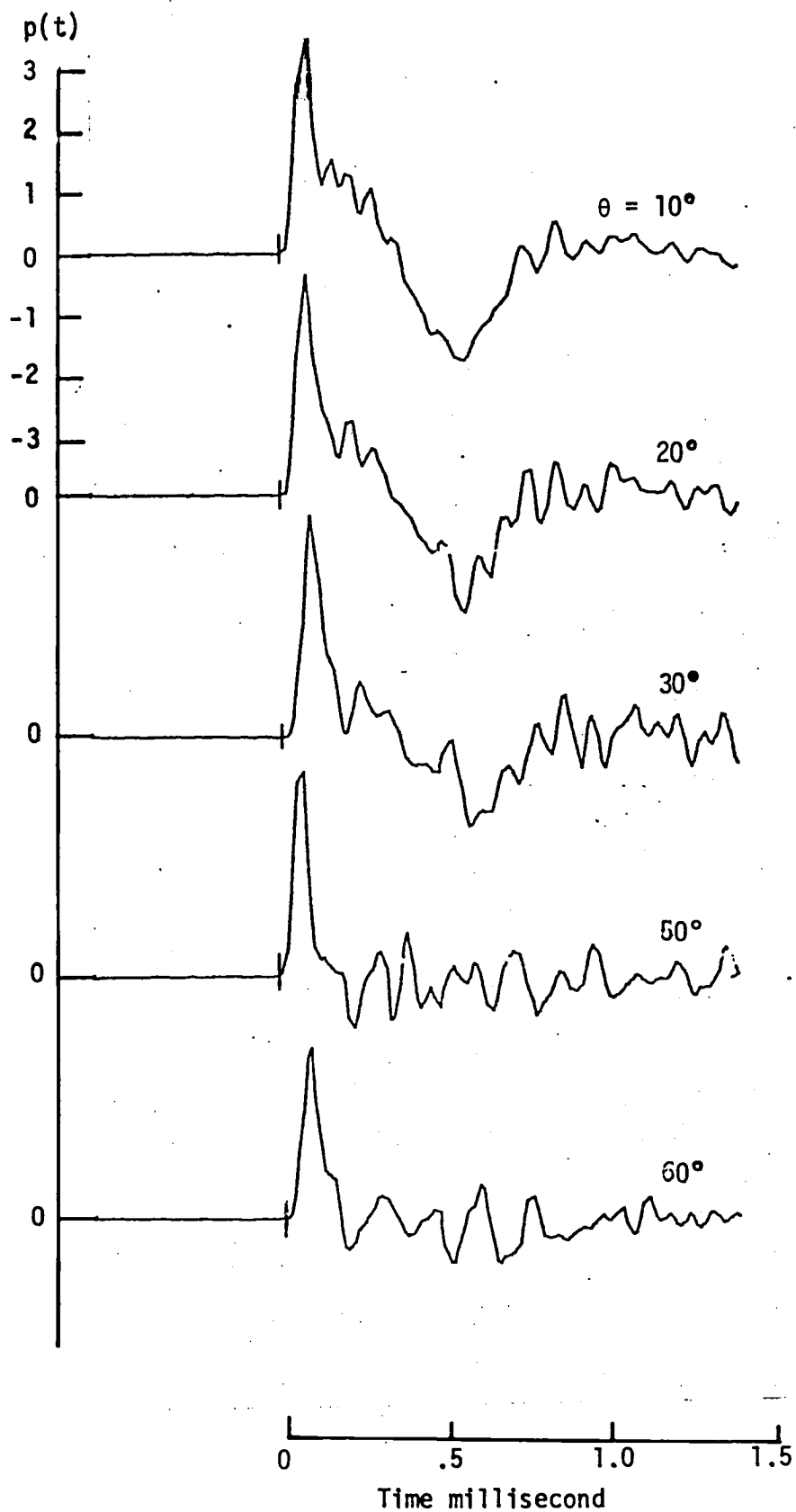


Figure 3a. Far-field pressure pulse without flow (experimental)

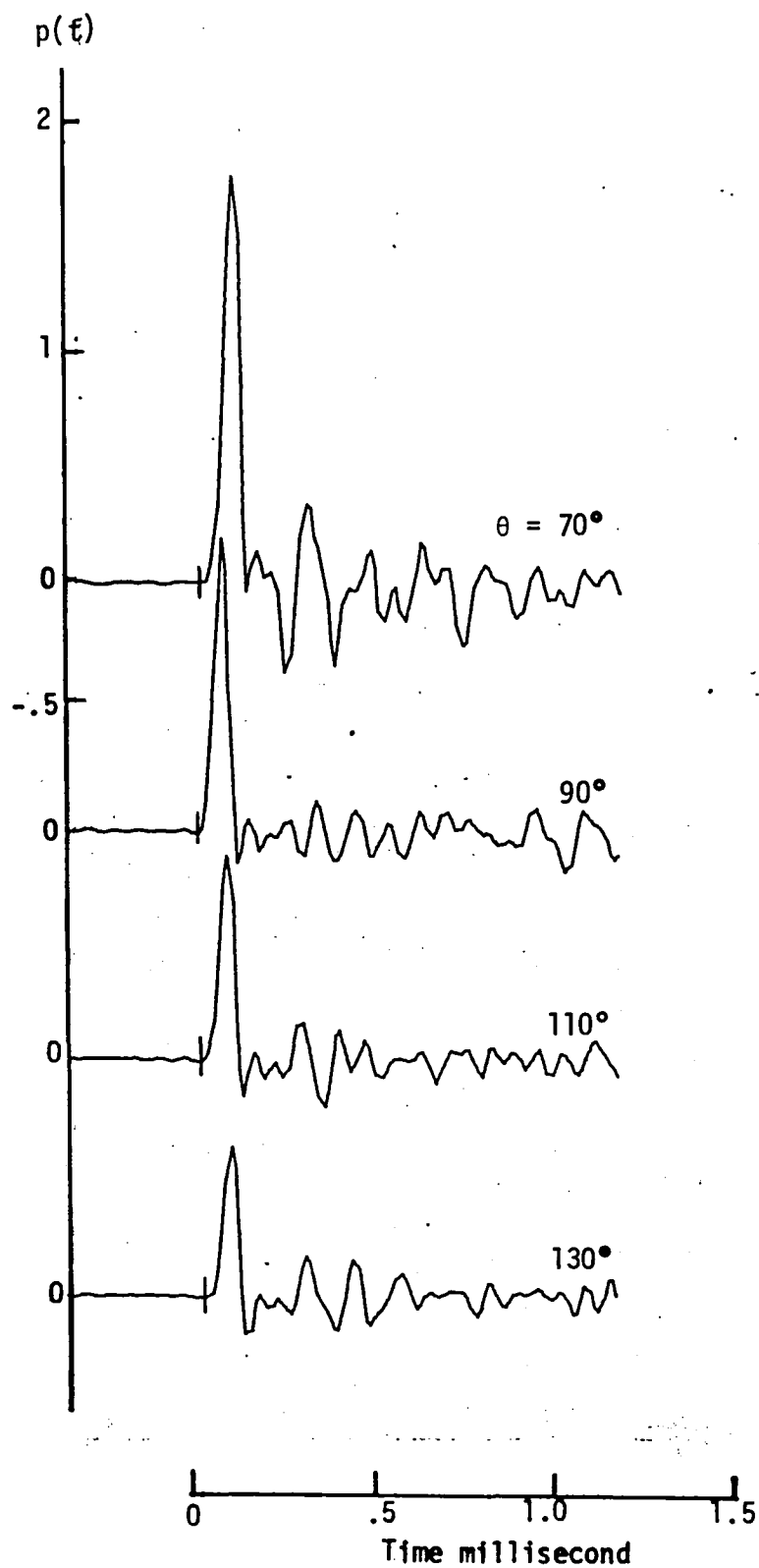


Figure 3b. Far-field pressure pulse without flow (experimental)

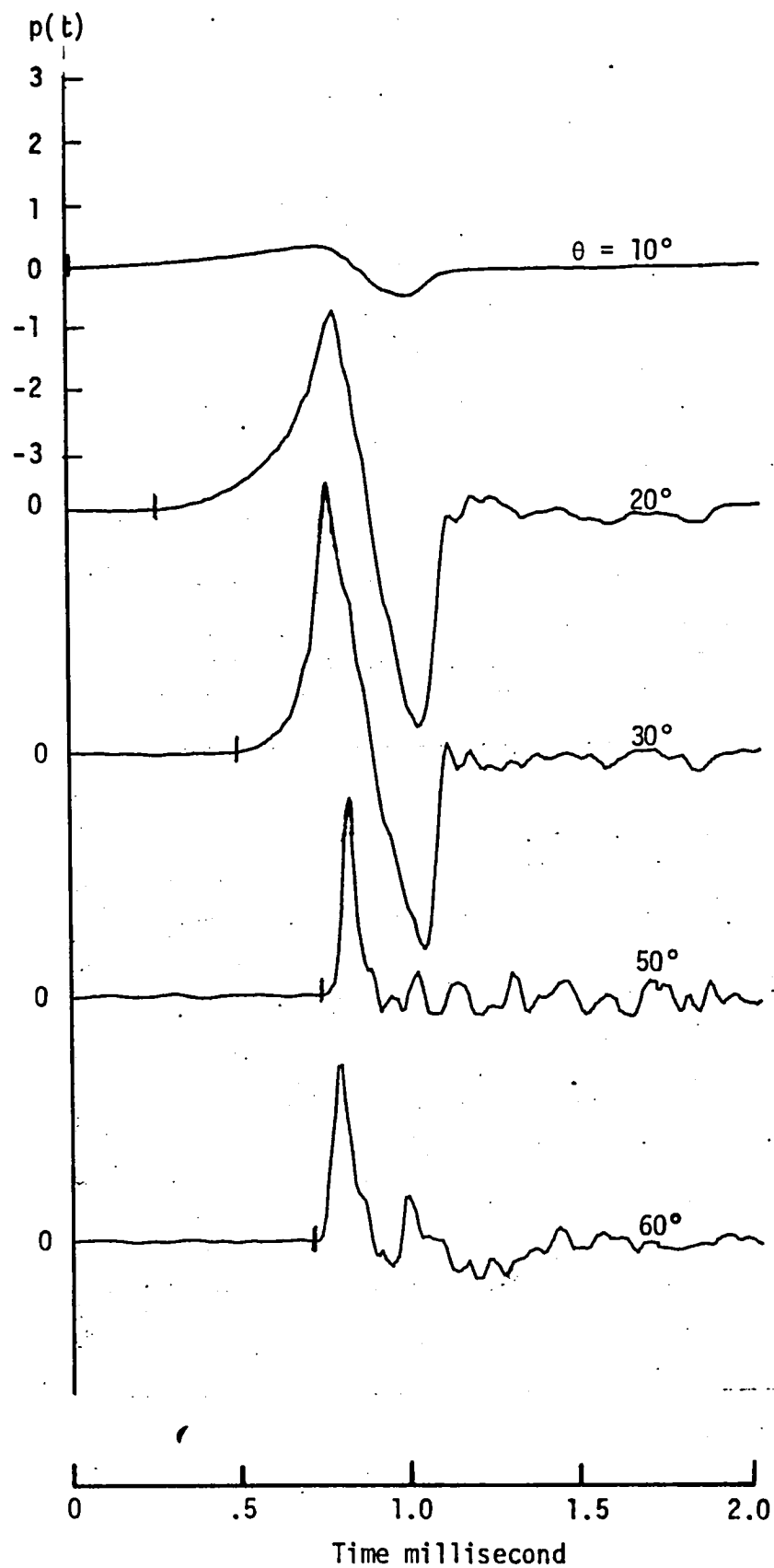


Figure 4a. Far-field pressure pulse with flow, $M = 0.66$ (experimental)

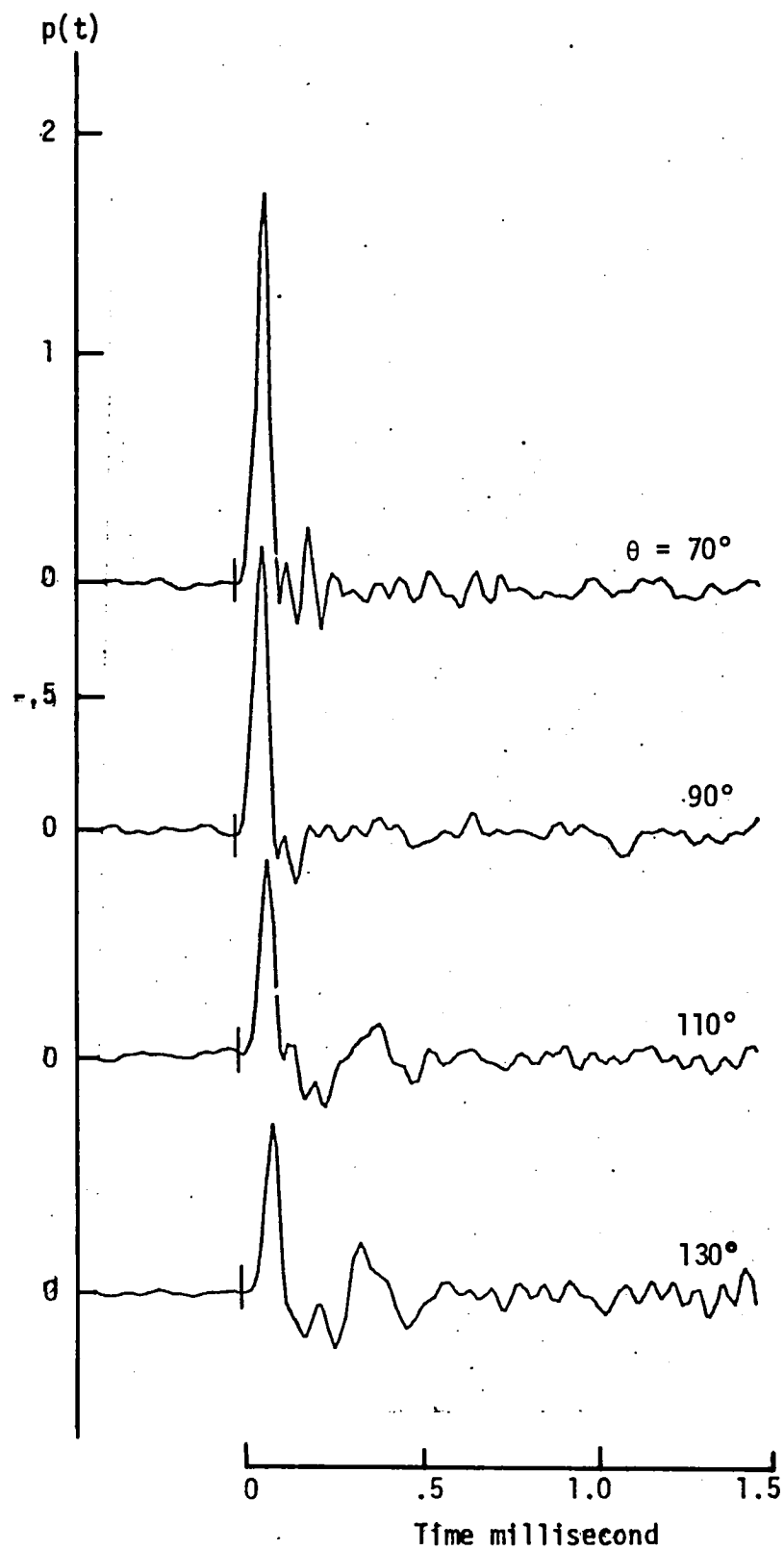


Figure 4b. Far-field pressure pulse with flow, $M = 0.66$ (experimental)

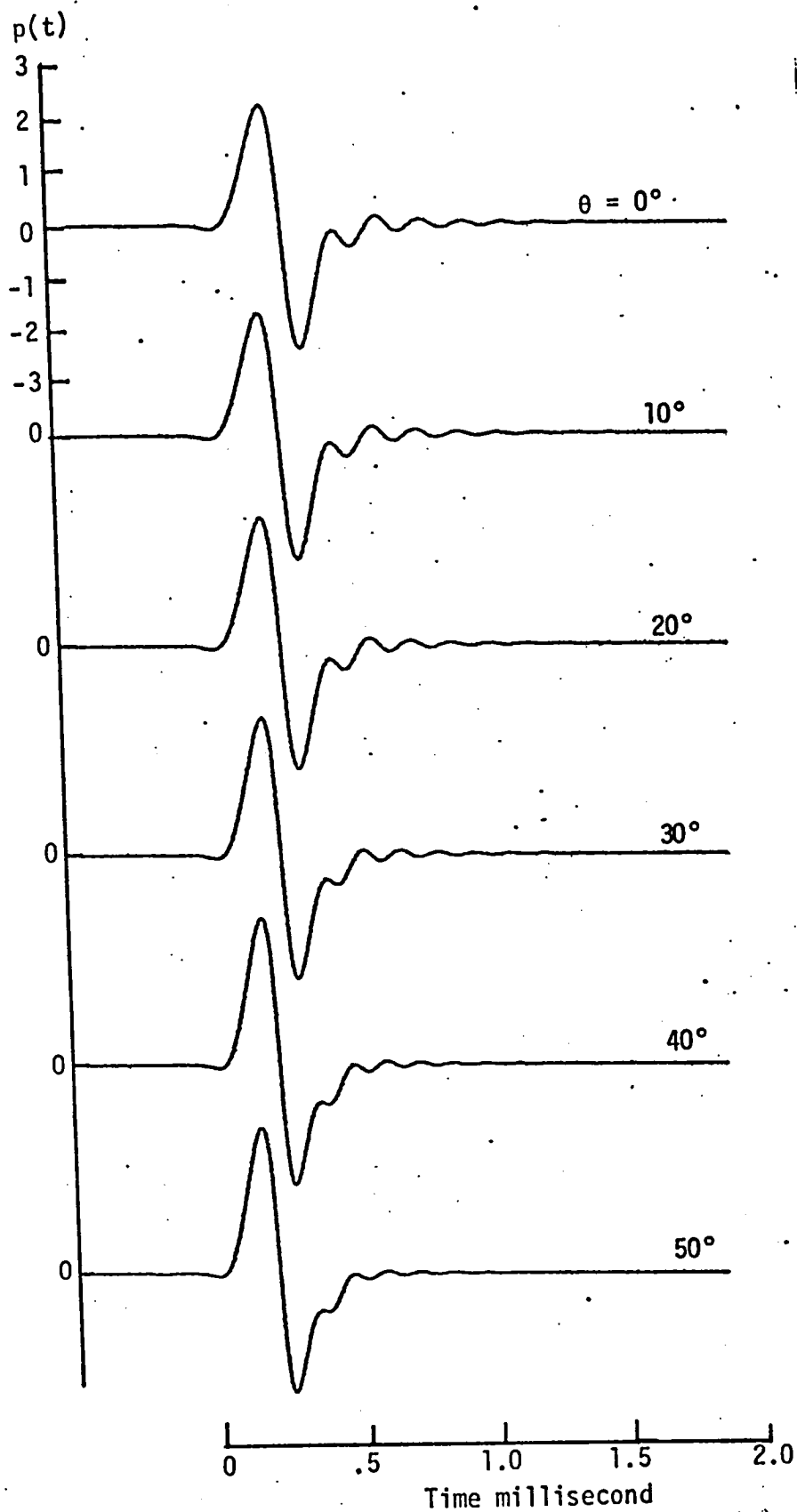


Figure 5a. Far-field pressure pulse without flow (numerical)

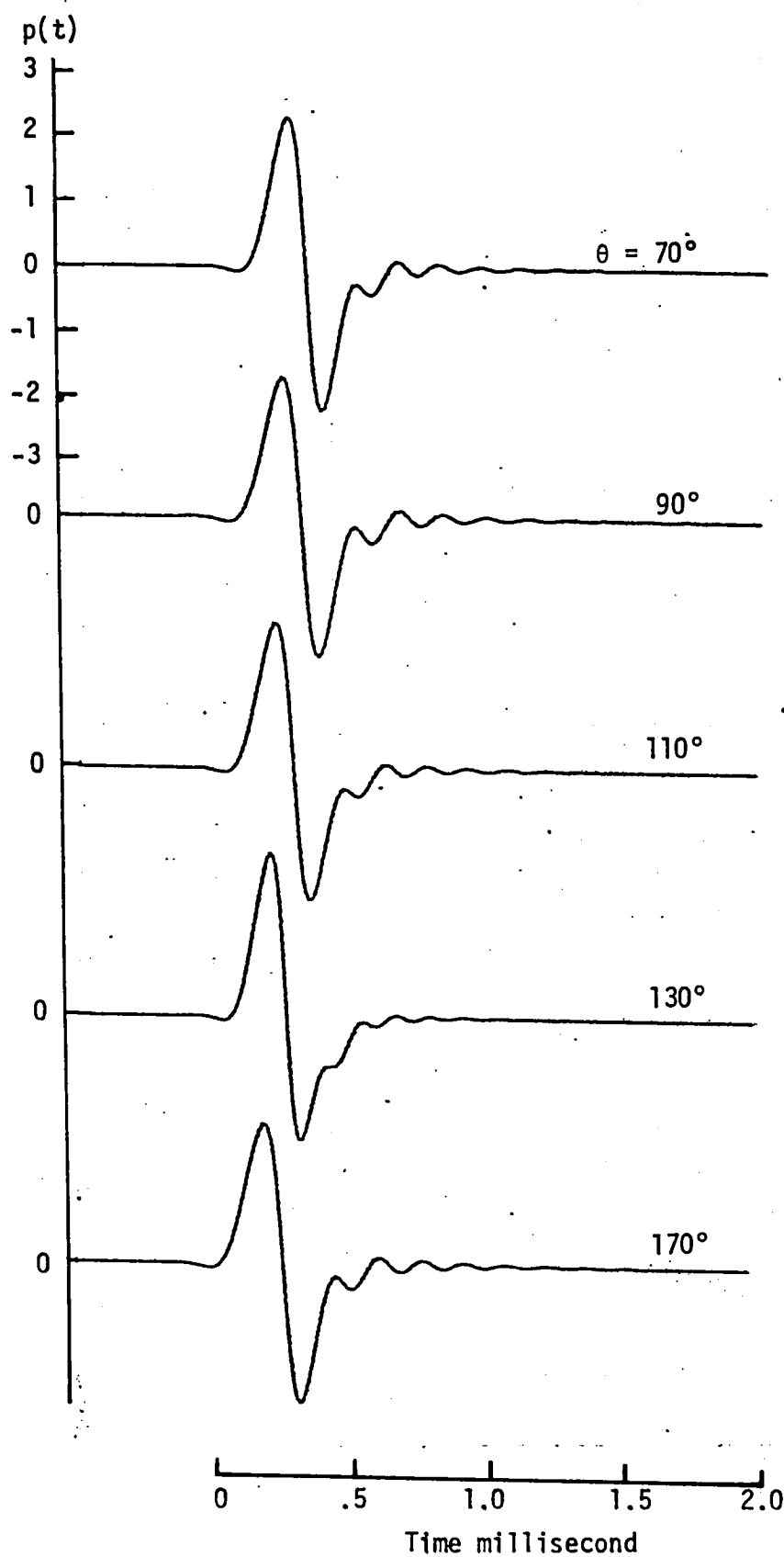


Figure 5b. Far-field pressure pulse without flow (numerical)

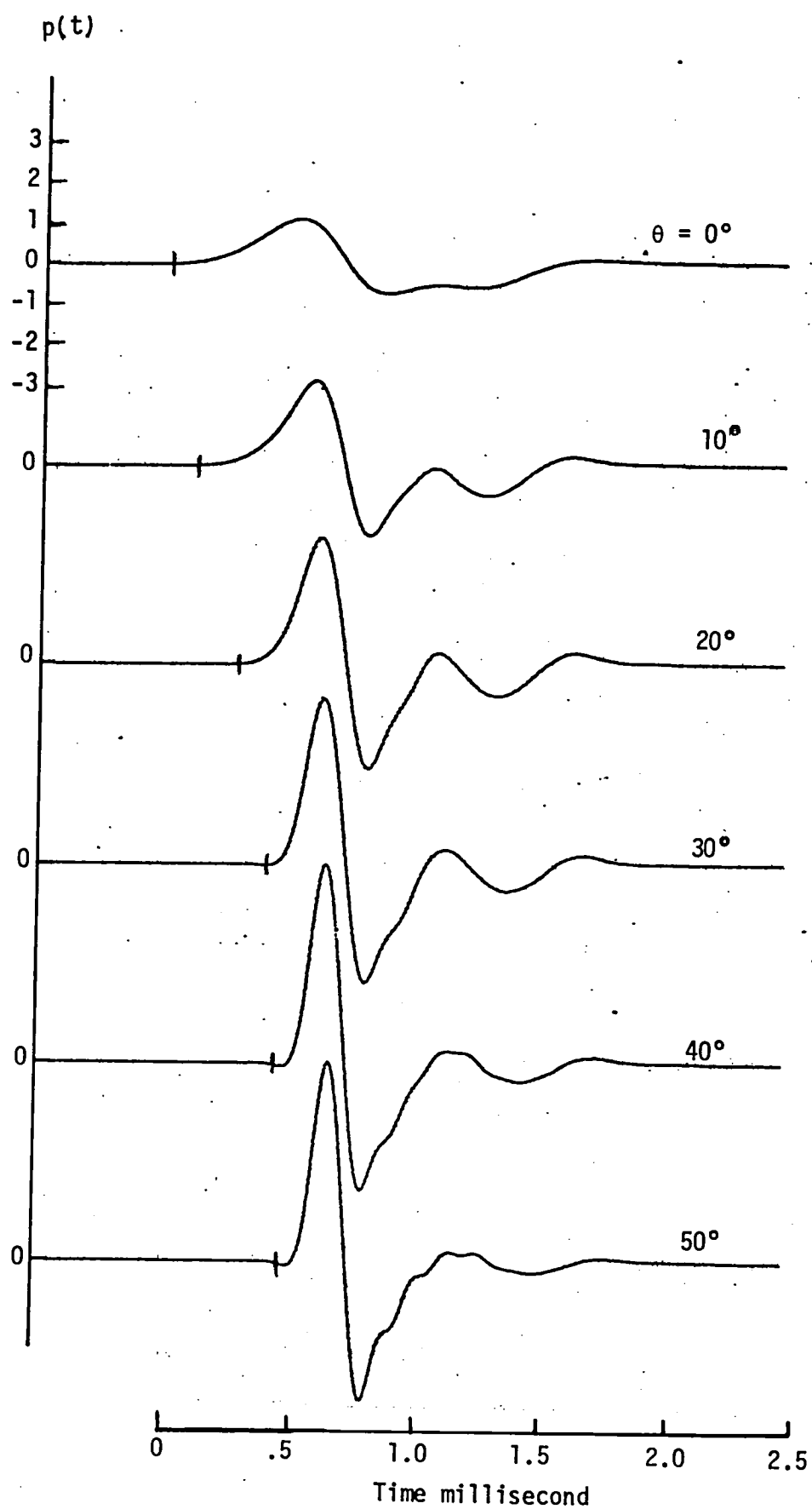


Figure 6a. Far-field pressure pulse with flow, $M = 0.66$ (numerical)

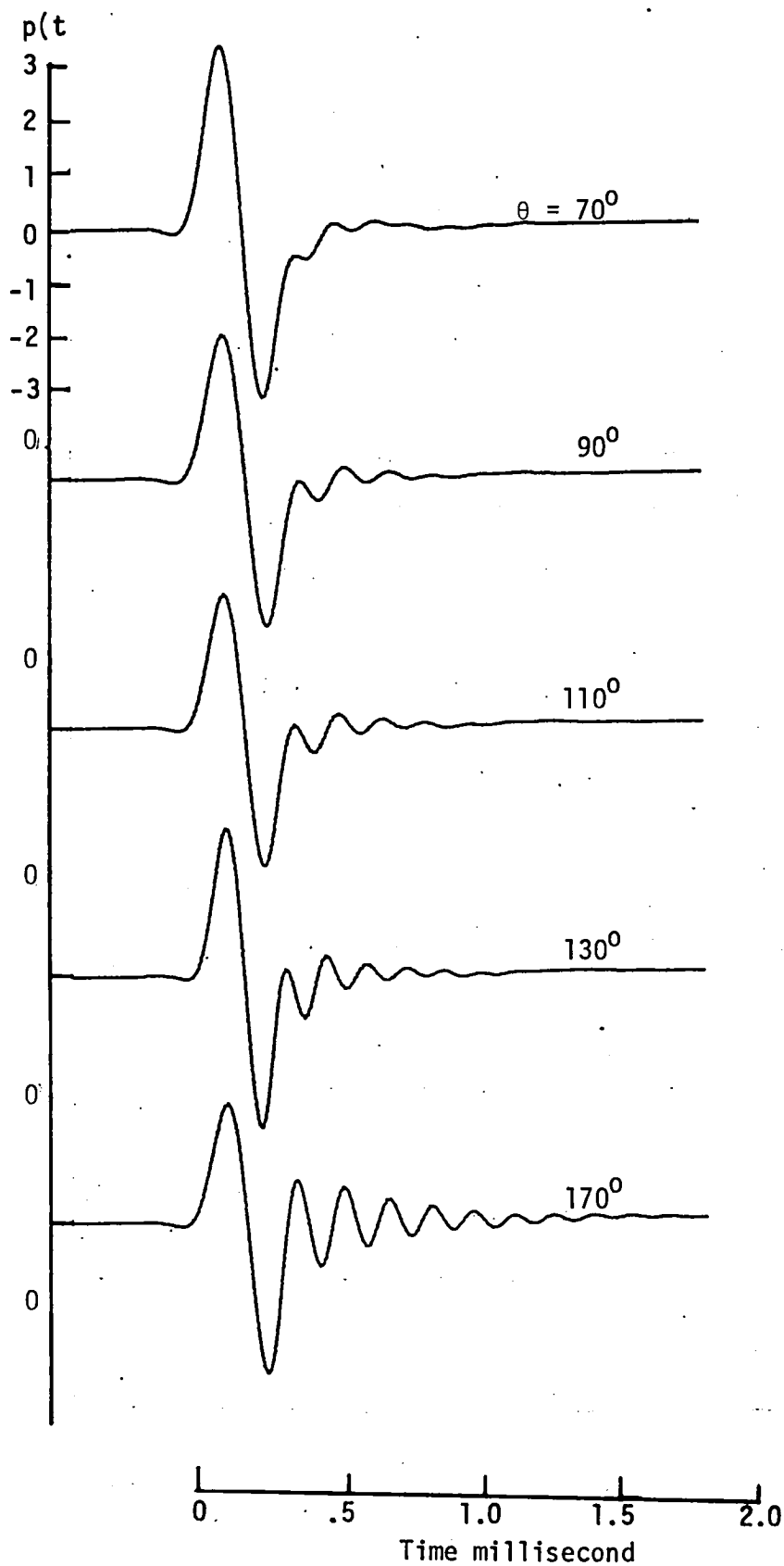


Figure 6b. Far-field pressure pulse with flow, $M = 0.66$ (numerical)

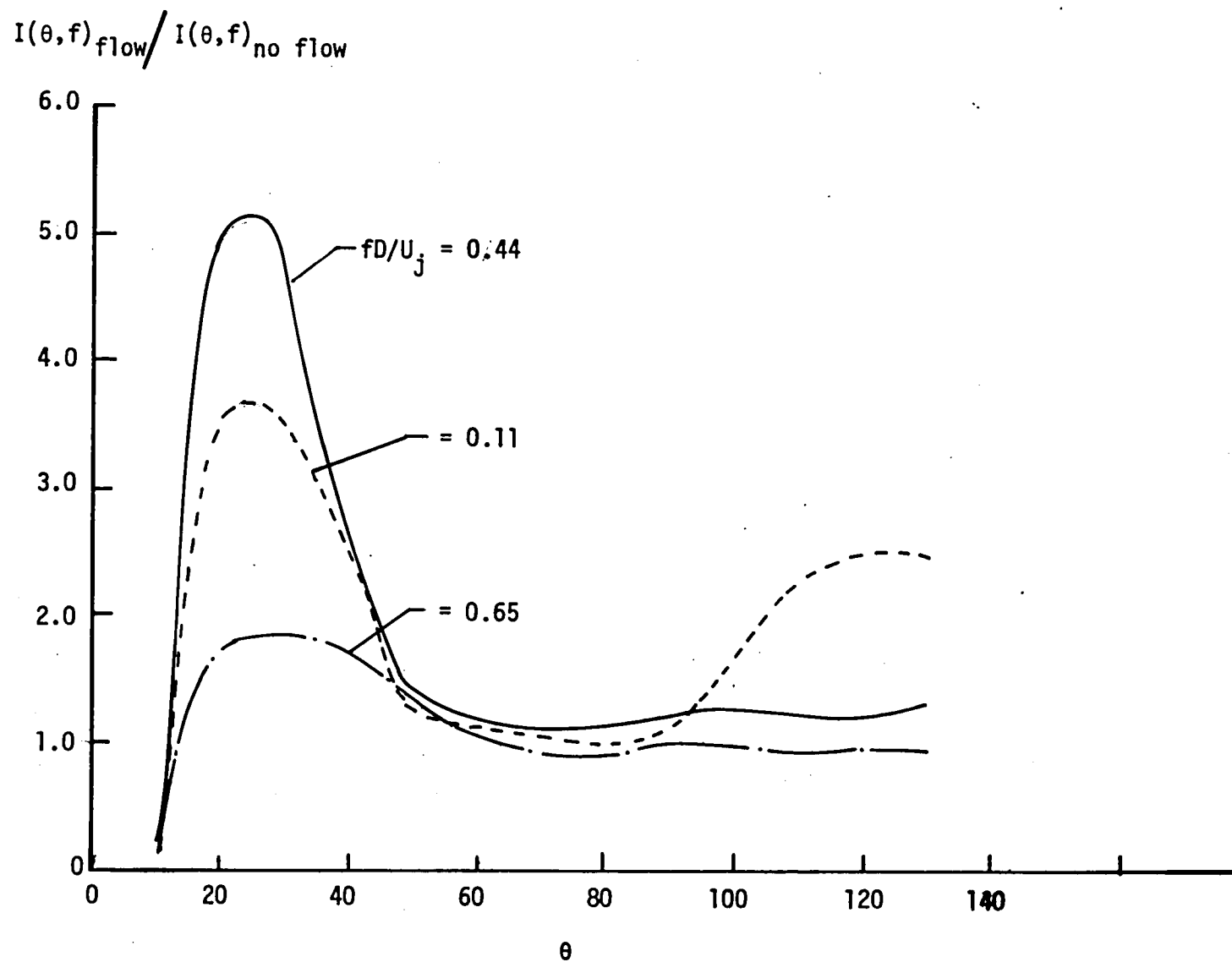


Figure 7a. Far-field intensity ratio of the pulse with and without flow, $M = 0.66$ (experimental)

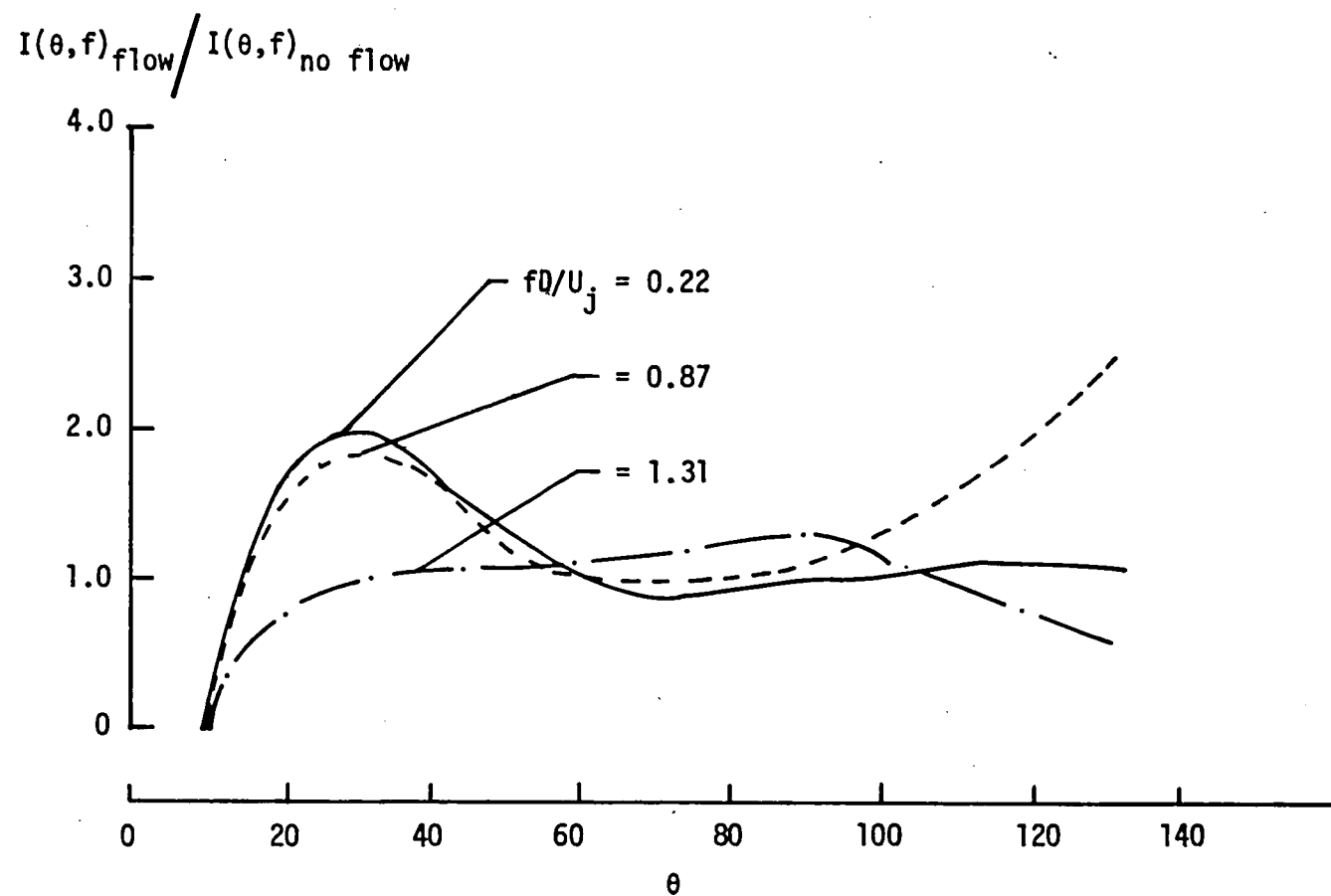


Figure 7b. Far-field intensity ratio of the pulse with and without flow, $M = 0.66$ (experimental)

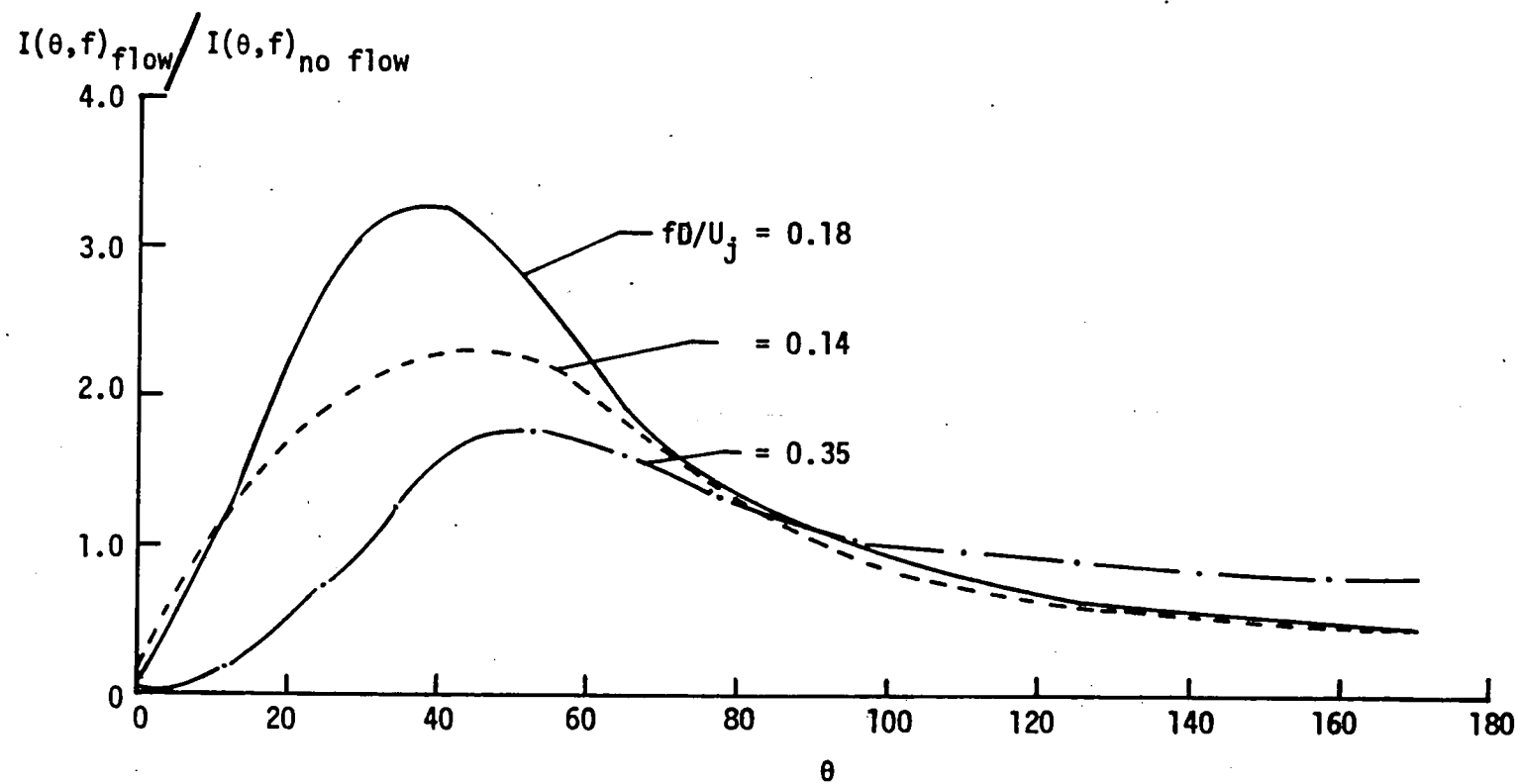


Figure 7c. Far-field intensity ratio of the pulse with and without flow, $M = 0.66$ (numerical)

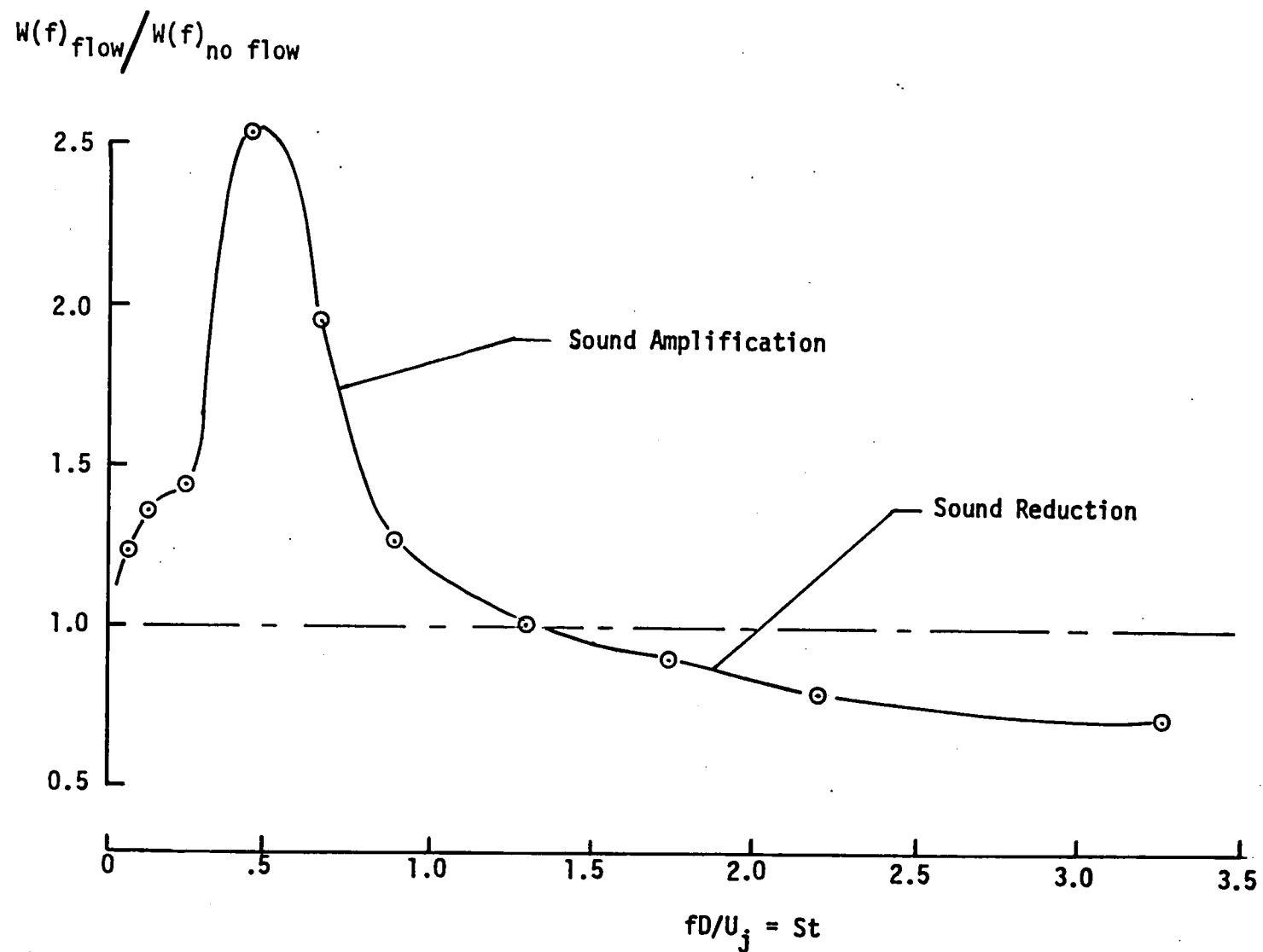


Figure 8a. Acoustic power ratio of the pulse with and without flow, $M = 0.66$ (experimental)

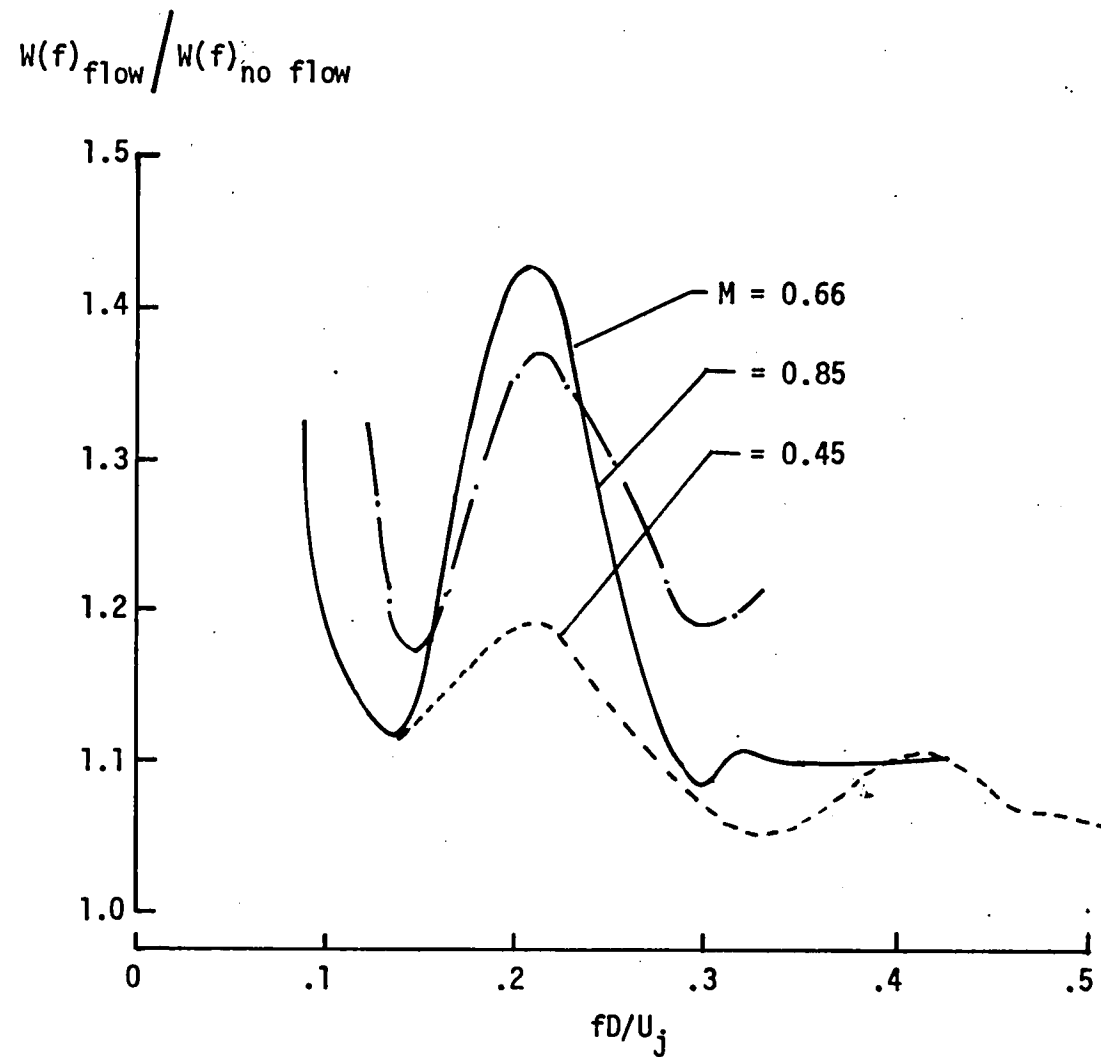


Figure 8b. Acoustic power ratio of the pulse with flow and without flow (numerical)

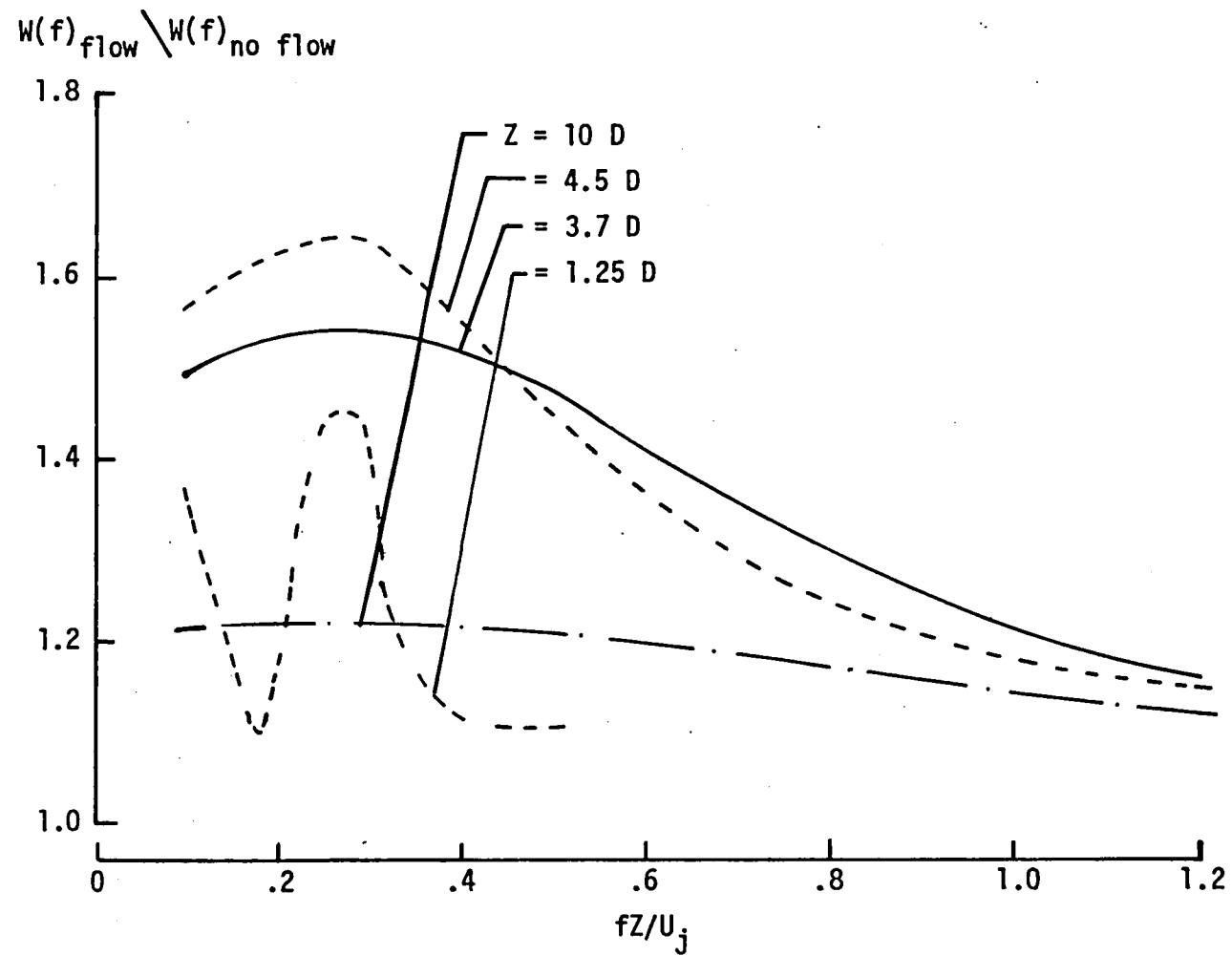


Figure 9. Amplification rate for different source position, $M = 0.66$ (numerical)

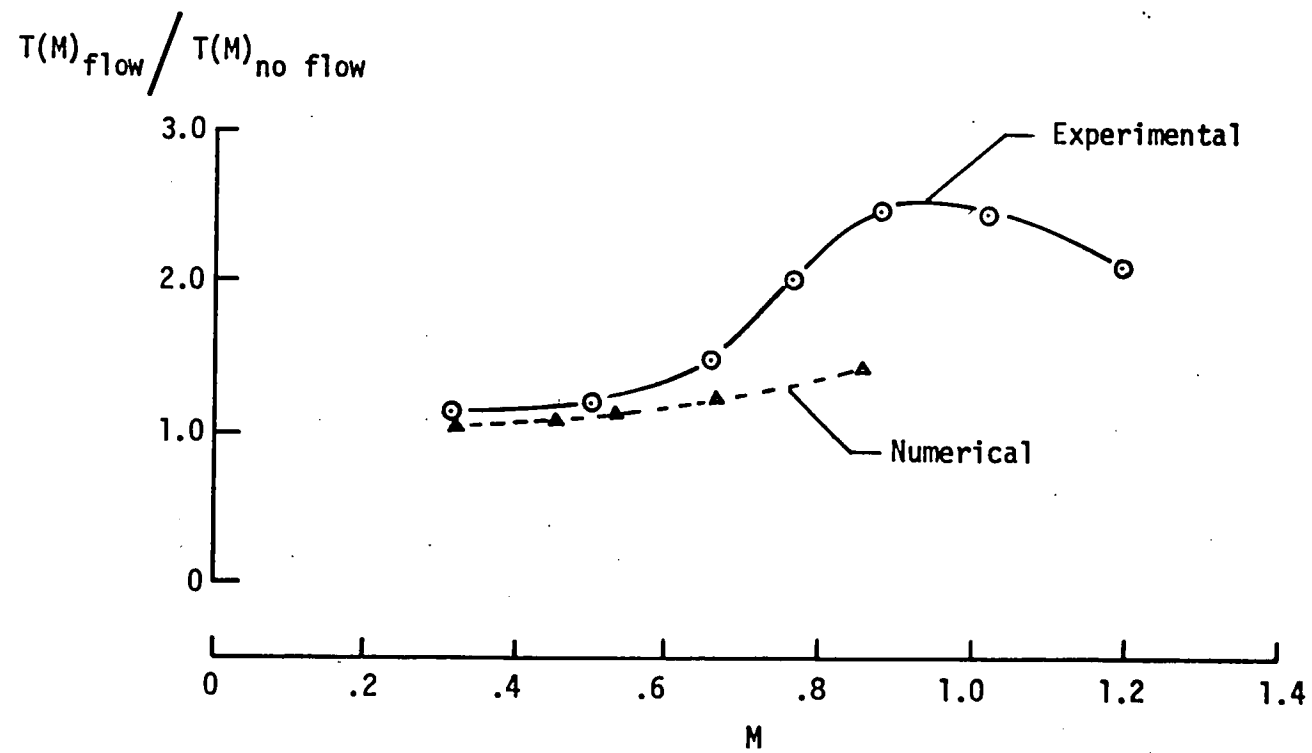


Figure 10. Variation of the total acoustic power ratio with flow Mach number

1. Report No. NASA TM 80183		2. Government Accession No.		3. Recipient's Catalog No.	
4. Title and Subtitle Experimental and Numerical Results on a Shear Layer Excited by a Sound Pulse				5. Report Date November 1979	
				6. Performing Organization Code	
7. Author(s) Lucio Maestrello, Alvin Bayliss*, and Eli Turkel*				8. Performing Organization Report No.	
9. Performing Organization Name and Address NASA Langley Research Center Hampton, VA 23665				10. Work Unit No. 505-32-03-05	
				11. Contract or Grant No.	
12. Sponsoring Agency Name and Address National Aeronautics and Space Administration Washington, DC 20546				13. Type of Report and Period Covered Technical Memorandum	
				14. Sponsoring Agency Code	
15. Supplementary Notes To be presented at the 32nd Am. Phys. Soc. Meeting in Notre Dame, Indiana, November 18-19, 1979 * Institute for Computer Applications in Science and Engineering (ICASE)					
16. Abstract The behavior of a sound in a jet is investigated both experimentally and numerically. It is verified that the far-field acoustic power increased with flow velocity for the lower and medium frequency range. Experimentally, an attenuation at higher frequencies is also observed. This increase is found numerically to be due primarily to the interactions between the mean vorticity and the fluctuation velocities. Spectral decomposition of the real time data indicates that the power increase occurs in the low and middle frequency range, where the local instability waves have the largest spatial growth rate. The connection between this amplification and the local instability waves is discussed.					
17. Key Words (Suggested by Author(s)) Jet noise Sound amplification Shear layer			18. Distribution Statement Unclassified - Unlimited Subject Category 71		
19. Security Classif. (of this report) Unclassified		20. Security Classif. (of this page) Unclassified		21. No. of Pages 45	
				22. Price* \$4.50	

